EXPLORING THE RELATIONSHIP BETWEEN LAND USE/LAND COVER TYPE AND WET-BULB GLOBE TEMPERATURE

A THESIS

SUBMITTED TO THE GRADUATE SCHOOL

IN PARTIAL FULFILLMENT OF THE REQUIREMENTS

FOR THE DEGREE

MASTER OF SCIENCE

BY

CALEB SAYLOR

DR. PETRA ZIMMERMANN – ADVISOR

BALL STATE UNIVERSITY

MUNCIE, INDIANA

DECEMBER 2017

Acknowledgements

I would like to thank my advisor, Dr. Petra Zimmermann, for her guidance and support throughout my research. I would also like to thank my other committee members, Dr. Adam Berland and Dr. Nathan Hitchens for the insight they have provided me with to complete my research. A special thanks also goes to fellow graduate student Jacob Rendall in the Department of Mathematics at Ball State University for helping me with finding the Excel macro that was desperately needed to complete my research. Thank you to the all of the professors of the Department of Geography at Ball State University for helping me and sharing their knowledge with me during my time there. I would also like to thank all of my friends, from grad school and elsewhere, along with my family for supporting me throughout the journey.

Table of Contents

I. Introduction

For some within the meteorology and climatology communities, keeping the public safe and informed are the top priorities. The need to know how the land and atmosphere interact with one another is just one of the many ways in which those priorities can be met. However, the atmosphere is fickle and chaotic, with even the minutest change potentially creating vastly different outcomes than expected. With the climate changing, some of these feedbacks may change or become exacerbated. One of these land-atmospheric interactions may magnify temperature. It is known that urban areas experience higher temperatures than rural or forested areas, especially in the evening (Gallo et al. 1996). This may be due to the amount of non-permeable surfaces in urban areas versus soil, with soil holding more moisture and thus having more moisture in the air above the surface. Changing the type of surface will thus change the amount of moisture in the air and the air temperature itself. This may cause the frequency of high temperatures to increase as well.

Temperature and atmospheric moisture play a large role in the heat stress of humans, along with radiation sources. These variables are often studied with reference to land cover type. However, the impacts on human life warrant greater consideration. It is understood that if temperature increases, Heat Index, which is the most commonly used heat-stress index in the United States, increases as well and that directly affects humans. Unfortunately, the Heat Index is only used in a few countries; even in those countries, some industries do not use it as a measure of heat stress. The Wet-Bulb Globe Temperature (WBGT) is used throughout most of the world and is commonly used in industries such as construction, military, and athletics in order to measure the heat stress on humans. However, how WBGT could vary with differing land cover types is overlooked. Also, the WBGT is often not measurable in situations where

money is an issue because the measuring device can be expensive and time consuming to use. The estimation of WBGT is then used in lieu of actually measuring it.

The purpose of this study is to investigate changes in estimated WBGT with different land cover types. Despite its wide use, WBGT is seldom studied in terms of atmospheric characteristics when comparing with land-atmospheric interactions, but it's used in specific situations that can help protect the health and safety of people. However, knowing how land cover type affects heat stress on humans could potentially save the lives of those who live or work in such extreme temperature conditions.

II. Literature Review

2.1 Heat-Related Illnesses and Deaths

With the continually changing climate, the frequency of extreme heat events (EHEs), which is defined by Anderson and Bell (2011) as "≥ 2 days with temperature > 95th percentile for the community for 1 May through September 30," are likely to increase according to the United States Environmental Protection Agency (2016a) and Pryor et al. (2014). Additionally, the consequences of EHEs will be exacerbated. Those include both heat-related illnesses (heat rashes, heat cramps, heat exhaustion, and heat strokes) and deaths. Data collected from 23 states between 2001 and 2010 found over 28,000 instances in which an individual was hospitalized due to heat-related illnesses, with rates ranging from 1 to 4 per 100,000 people; the highest rates occurred in the Midwest and Southeast United States (EPA 2016a). Death rates from 1974 to 2014 were ten times less than heat-related illnesses between 2001 and 2010. The average death rate between 1974 and 2014 ranged from 0.5 - 1 deaths per 1,000,000 instances, which corresponds to approximately 9,000 deaths (EPA 2016b). However, the number of deaths due to prolonged heat exposure are potentially higher due to both heat-related deaths not being correctly identified on death certificates and/or not being identified as the underlying cause of death by medical professionals. When heat is identified as both an underlying cause and a contributing cause of death, the rate nearly doubles. In one study, it was found that death rates due to prolonged heat exposure were higher in the Midwest and Northeast (Anderson and Bell 2011). This may be linked to non-acclimatization of the populace.

Using data collected from the Centers for Disease Control and Prevention (CDC), the EPA (2016b) was able to identify heat as the leading cause of death among weather-related phenomena. The risk for over-exposure to heat can be mitigated by taking appropriate measures,

including limiting exposure time, remaining hydrated, being knowledgeable about various work strain safety thresholds, and knowing if someone is a person who is "at risk." The problem of preventing heat-related illnesses and deaths during EHEs is a public issue as well, with cities often constructing "cooling centers" where the public can go to gain relief. The danger for heat-related illnesses and deaths in not just a phenomenon limited to the outside atmosphere either; industries in which people work in closed spaces in a hot environment, such as steel mills, are concerned about heat-related illnesses and deaths as well.

The heat can be very dangerous, but some people still do not take it into serious consideration when engaging in physical activities outside. For example, a 14 year-old student at Pike High School in Indianapolis, Indiana, passed away during football practice from "heat stroke due to hyperthermia" (Wierks 2015). Although most are cognizant of the risks of EHEs, there are still incidents where the proper precautions are not taken.

2.2 Heat-Stress Indices

One way to identify the precautions needed to be taken during an EHE (or when conditions are hot and humid in general) is by knowing about various heat-stress indices. A heat-stress index is a single numerical measurement which provides information about the conditions of the atmosphere with reference to the actual air temperature. Most heat-stress indices use multiple data inputs in order to assess how the atmosphere will affect humans. Multiple studies have been conducted in order to create a heat-stress index for the primary use of measuring/estimating the heat stress experienced by humans (Bröde et al. 2012; Moran et al. 2001a; Thom 1959). Heat stress occurs when the body struggles to cool itself through transpiration, but the effects can differ for individuals. It is a function of thermoregulation of the human body as a whole, which is outside of the scope of this research. Macpherson (1962)

summarized various heat stress indices, some of which are still in use today. Arguably, the most important component of the measure of heat stress, while not necessarily a heat stress index in and of itself, is the dry-bulb temperature. The dry-bulb temperature is simply the air temperature recorded by a dry-bulb thermometer. This is in contrast to the wet-bulb temperature, which is recorded by a bulb thermometer with a water-soaked sleeve covering the bulb. The wet-bulb temperature can be thought of as a heat stress index because it takes into consideration both the air temperature and the relative humidity. Its use as a heat stress indicator was the result of research of work conditions of mines in Cornwall, United Kingdom, in the early 1900s (Macpherson 1962).

2.2.1 Effective Temperature

One of the first widely used heat stress indices was developed in the 1920s and was known as the Effective Temperature. It was a measure of the combined effects of air temperature, humidity, and wind speed. The way it was created was described by Macpherson (1962) as follows

> "The temperature and humidity in one test chamber were adjusted until the degree of comfort or discomfort experienced was judged by a small group of trained observers to be equal to that experienced in an adjacent test chamber maintained at a different temperature and humidity. Combinations of dry- and wet-bulb temperature satisfying this requirement were plotted on a psychrometric chart and through them a line of equal comfort was drawn. The intersection of this line with the dew point line defined the effective temperature of all such combinations."

The Effective Temperature had two scales: (1) normal, which took into consideration a human who was wearing normal inside clothes and (2) basic, which took into consideration a human who was clothed from the waist down. The effective temperature was the most widely used measure of human comfort for many decades following its introduction. In the 1930s, the globe-thermometer temperature came along. The device, a thermometer inside a 6-inch hollow copper sphere painted black, was introduced to help measure the effects of the air temperature,

wind speed, and mean radiant temperature had on thermal comfort. The uniform temperature of an imaginary black enclosure results in the same radiational heat loss from a person as the actual enclosure. The aforementioned indices were known as "indices based on measurement of physical factors" due to the fact that they "provide no direct measure of physiological effect" (Macpherson 1962) and although not used as standalone measurements of heat stress today, they did lead to the development of the Wet-Bulb Globe Temperature, considered by Epstein and Moran (2006) as a "direct index" and one of the most widely used heat-stress indices throughout the world.

2.2.2 Wet-Bulb Globe Temperature

One widely used heat-stress index, the Wet-Bulb Globe Temperature (WBGT), was created to help limit the heat stress and injuries experienced by military trainees (Yaglou and Minard 1957). This heat-stress index is based on a prior study which measured metabolic heat loads of each of the various training exercises. The WBGT also used meteorological data that included the shaded dry-bulb and wet-bulb temperature (obtained from sling psychrometers), globe thermometer temperature used to account for effective radiation from every source, wind velocity measured by thermoanemoemeters, intensity of direct solar radiation and diffuse solar radiation using pyrheliometers, and mean radiant temperature of the sky and ground measured by radiation thermopiles. The authors then used the effective temperature index to combine temperature, humidity, radiation, and wind into a single value. The final version of the WBGT (the index used for outdoor assessment of the environment), was published in its final form by the Departments of the Army, Navy, and Air Force (1957). It considers only three variables: the shaded dry-bulb temperature (T_d), the natural wet-bulb temperature (T_w) and the black globe temperature (T_g) using the following formula

$$WBGT = 0.7*T_w + 0.2*T_g + 0.1*T_d \quad \textbf{(eq. 1)}$$

The black globe temperature, measured by a thermometer inside a 6-inch hollow sphere made of copper covered in the same olive-colored fabric as the uniforms worn by Marine Corps trainees, was included to measure radiation from all sources. It was found that the olive-colored uniforms had an absorptivity of 0.74, compared to the 0.95 for the black globe. Another device similar to the globe thermometer is the wet globe thermometer. As the name implies, it is simply a globe thermometer that is wet. Botsford (1971) explains that, like the globe thermometer which considers heat from both direct beam radiation and that radiated by surrounding surfaces, it also has the added effect of being cooled by evaporation via wind and humidity. He believes that this measurement simulates the ability for humans to thermoregulate in hot and humid conditions via sweating and that it is a good measure of heat stress, which correlates well with the WBGT. The wet globe thermometer became known as the Botsball (BB) and it was later found that if the estimations of wind speed, humidity and radiant heat were readily accessible, the BB could predict the WBGT within 0.4°C (Ciriello and Snook 1977). However, in environments with high temperatures (greater than 41°C), high wind, and constant relative humidity, the difference between the BB measurement of the Wet Globe Temperature and the WBGT varied by as much as 9°C in a desert-like climate (Gonzalez et al. 1985).

The WBGT is employed in various industries, and is the most widely used measure of heat stress today. The military still utilizes this measurement to see if it is safe for trainees to perform training activities. Many athletic organizations use the WBGT to assess whether it is safe to practice or play a match. For example, The Fédération Internationale de Football Association (FIFA), the global governing body of soccer, uses the WBGT to monitor atmospheric conditions during matches. Their health officials determined that if the WBGT

exceeded 32° C (89.6° F) throughout the match, additional water breaks were required during the match. However, no thresholds are set out for practices; those are the responsibility of each individual national soccer governing body. The International Olympic Committee had scientists review evidence and found that for non-aquatic events, the heat stress is dependent on the elements calculated in the WBGT (Bergeron et al. 2012). The Occupational Safety and Health Administration (OSHA) has its own set of guidelines for measuring heat stress using the WBGT. However, it is based both on the WBGT and the energy expenditure (in kcal) per hour of the average worker. Similar safety thresholds are set out by International Organization for Standardization (ISO) in ISO 7243:1989 (Standardization 1989), which also states a formula for calculating the WBGT for indoor environments. The outdoor WBGT is calculated using a weighted measurement of the WBGT taken at the head level of the individual, the abdomen, and the ankles. However, ISO 7243 states, "for rapid determination of the WBGT index, it is enough to carry out one measurement at the level where the heat stress is maximum" (Standardization 1989).

2.2.3 Apparent Temperature

Despite the wide use of WBGT, both early in its development and today, this did not signal the end of attempting to develop different heat stress indices. Another of these models, which was developed after Macpherson's (1962) work, is the Apparent Temperature. Steadman (1979a, 1979b) based his model on what he referred to as "sultriness," which is the combined effects of high air temperature and high humidity. Calling his single value the apparent temperature, Steadman (1979b) defined it as "the ambient temperature adjusted for variations in vapor pressure above or below some base value." These base values are

1. Vapor pressure = 1.6 kPa
2. Wind speed = 2.5 m s^{-1}
3. Barometric pressure = 101.3 kPa
4. Extra Radiation = 0

The Apparent Temperature was calculated for both mild and extreme conditions and took into consideration factors other than meteorological variables. Physiological characteristics such as the dimension of an average adult, core vapor pressure, and surface temperature and vapor pressures of skin, among others were considered in the development of this heat-stress index. Thermodynamic properties were also taken into consideration. These include, but are not limited to, surface convection, heat transfer from clothing, resistance to heat transfer of clothing, surface radiation, and the effect of the wind h on the heat-stress of a human. Steadman (1979a) knew that the ambient conditions played a large role in whether or not the wind was making humans feel warmer or colder. The chosen average wind speed was selected because "winds less than the base speed of 2.5 m s^{-1} are scarcely detectable by the average moving person" (Steadman 1979b).

Radiation is a problem which is mostly unavoidable to those outside, even those who are in the shade. Direct exposure to the sun is the main concern for heat-stress in humans, but upwelling longwave radiation can affect the apparent temperature, as absorption of upwelling longwave radiation by humans can reach 200 W m^{-2} (Steadman 1979a). This value is approximately half of the longwave radiation emitted from the earth's surface. The apparent temperature for a wide range of values of temperature, humidity, wind speed, and barometric pressure was calculated using knowledge of the planetary boundary layer, the physiological properties of humans, and clothing science. These were distilled into a single value, which is perhaps why it formed the basis of the most popular U.S. heat-stress index, the Humitrue, developed in 1978 by WJXT (Jacksonville, Florida) broadcast meteorologist George Winterling.

His index was then adopted by the National Weather Service (NWS) and named the Heat Index (HI). The U.S. HI differs from the Canadian HI, namely because the U.S. HI considers heat balance rather than just vapor pressure. However, Santee and Wallace (2005) found that both are correlated with the predicted rectal temperatures of humans, which is another physiological measure to predict heat stress (Santee and Wallace 2005).

2.2.4 Universal Thermal Climate Index

More modern heat-stress indices have been developed to either estimate the WBGT or replace it entirely. One of these is the Universal Thermal Climate Index (UTCI) (Jendritzky et al. 2008), which incorporates both physiological response of the body and various meteorological and environmental inputs founded on a baseline environment with 50% relative humidity (RH) and vapor pressure limited to 20 hectopascals (hPa). The index uses meteorological variables such as air temperature, atmospheric pressure, wind speed, water vapor, and solar radiation inputs such as shortwave and longwave radiation fluxes. Metabolic heat load on the body and clothing insulation are also included in the calculated of the UTCI.

The operation of calculating the UTCI was then simplified by Bröde et al. (2012) to limit the computational power needed to calculate the UTCI in climate models. With heat-stress being a factor in athletics, Brocherie and Millet (2015) believe that the UTCI is a more useful heat-stress index for athletes due to their belief that it better represents physiological response to hot environments. The Required Sweat Rate model used in ISO 7933:2004 (Standardization 2004) was used to estimate the thermoregulation of humans working in hot environments by taking into consideration environmental conditions and clothing worn by a human, among other factors. However, it was suggested by Malchaire et al. (2000) to change the criteria of ISO 7933:2004 to consider the physiological factor of an increase in the temperature of the core with activity

during “normal conditions.” The Predicted Heat Strain model was found to improve the prediction of sweat rate, and thus acceptable extreme heat exposure time (Malchaire et al. 2001).

2.2.5 (Modified) Discomfort Index

The Discomfort Index (DI) created by Thom (1959) was one of the first widely used heat-stress indices. The index considered both the dry-bulb temperature and the wet-bulb temperature and was constructed because effective temperature was not easily calculated from standard observations. The DI was then adjusted by Sohar et al. (1962), which resulted in a simpler DI formulation. Moran et al. (1998) compared the results of DI and the Wet-Bulb Globe Temperature (WBGT) from 3 different weather stations in the world. The DI was modified by calculating a new linear relationship between collected data. This was done because with higher values of WBGT and DI, the deviation from the mean line between WBGT and DI grew larger. Moran et al. (1998) found that the Modified Discomfort Index (MDI) did a better job of estimating heat-stress on a human rather than replacing the WBGT all together. Another study (Moran and Pandolf 1999) was done comparing the MDI to the WBGT and DI to assess the importance of the Globe Temperature (T_g) in the calculation of heat stress. It was found that MDI had a significant correlation with WBGT, and since it did not use T_g, it was simpler and thus better to use as an indicator of potential heat stress.

2.2.6 Environmental Stress Index

Another heat-stress index (Environmental Stress Index) was created by Moran et al. (2001a) in order to find an alternative to the WBGT. Using multiple regression analysis and data collected from three different climate types, Moran and Pandolf (1999) constructed various models for the WBGT that were dependent on air temperature (T_a), relative humidity (RH), and solar radiation. It was found that ESI also correlates well with WBGT and could be used as a

substitute due to the use of more accurate micro-sensors employed to measure atmospheric conditions. The ESI was evaluated by Moran and Epstein (2006) with data obtained from different databases used to construct ESI, and the results showed once again that ESI was highly correlated with the WBGT, and thus a good substitute for it for the same reasons as Moran and Pandolf (2001) explained in the creation of ESI.

2.2.7 U.S. Army Research Institute of Environmental Medicine

Many of the heat stress indices that have been developed have been focused on use for the general public. However, heat-stress experienced by military personnel has been a pressing topic of the United States government for decades, as evidenced by the development of WBGT in the 1950s. The U.S. Army Research Institute of Environmental Medicine (USARIEM) developed its own heat-strain model (Army Research Institute of Environmental Medicine (ARIEM)) used to predict physiologic strain (body temperature, heart rate, and sweating rate), specifically for military personnel who have to wear various levels of Mission Oriented Protective Posture (MOPP) gear (Cadarette et al. 1996). The MOPP gear levels were each assigned correction values to be added to observed WBGT when heat-stress is a concern. Another study calculated adjustment values for different, more normal clothing ensembles by calculating the core temperature of the study subjects (Bernard et al. 2008). Other models constructed by the USARIEM (e.g. Heat Strain Decision Aid (HSDA) and ARIEM-EXP) were able to predict core temperatures, which are used as a physiological estimation of heat-stress on humans (Cadarette et al. 1999). The AIREM model has also been modified for use in high altitude environments and has done well with predicting the heat stress in such locations, showing that evaporative skin cooling increases with altitude (Matthew et al. 2003).

However, one problem with all of these heat-stress indices, with exception of Required Sweat Rate model and WBGT, is that they do not have their own internationally recognized and utilized workload safety thresholds. Having the safety thresholds backed by physiologic research is pivotal to providing proper guidance in preventing heat-related illnesses and deaths. This is perhaps one of the reasons why WBGT is so widely used throughout the world. However, WBGT does have its limitations. These limitations include, but are not limited to, belief that WBGT does not respond as quickly as do changes in atmospheric conditions (Moran et al. 2001a), that its use in a broad range of scenarios where the black-globe temperature is needed limits its accuracy (Epstein and Moran 2006), and that the calibration of devices to measure WBGT is inadequate (Budd 2008).

One of the biggest problems with WBGT calculation is that it is quite cumbersome to compute. The device used to gather the necessary data is expensive and time consuming to use, and thus is not utilized by smaller organizations such as schools and small construction companies. That is why it has been important to estimate the individual components of the WBGT, primarily T_w and T_g. One of the primary concerns is those workers who work inside environments that can become extremely hot, chief among them aluminum smelters. A number of studies have been conducted to estimate WBGT inside buildings that house aluminum smelters (Akbar-Khanzadeh and Ramsey 1987; Bernard and Pourmoghani 1999; Dernedde and Gilbert 1991; Lemke and Kjellstrom 2012; Plunkett and Carter 1974). Most of these found that WBGT inside the building can be closely predicted, whether it be by the use of including outdoor measurements in an environment that is open to the outdoors, using empirical models, or thermodynamic models. However, Plunkett and Carter (1974) believe WBGT is not appropriate to use inside aluminum smelter plants due to a large amount of data needed from multiple

locations throughout the building in order to calculate a time-weighted average WBGT. Naturally, this issue could be extended to include other hot, indoor environments as well, such as steel mills. Another issue with using WBGT indoors is the estimate is more accurate further away from the furnaces, but WBGT is higher closer to it, which is obviously not beneficial (Emes et al. 1978). These findings are in contrast to those of Dernedde and Gilbert (1991), who discovered in their study area that there was less than a 3% difference between the predicted and observed values of WBGT.

Another concern of heat-related illnesses and deaths is those who are outdoors in extreme heat. The WBGT is tedious to calculate using the standard measuring devices. That is why attempts to estimate the components of WBGT using other methods have been made. One such method uses Heat Index and Adjusted Temperature to estimate WBGT. Employing the empirically derived formula provided by Bernard and Iheanacho (2015), the Heat Index value can help provide an estimate of WBGT within ±2°C. In comparison, using Adjusted Temperature provided an estimated WBGT between 1°C below and 1.4°C above the actual WBGT. However, it was determined that using Heat Index or Adjusted Temperature did not provide an estimate for the actual WBGT within 1°C, and thus is not recommended for use. Another method used a 50 mm globe instead of the standard 150 mm diameter black globe thermometer. It has been shown that using the 50 mm globe provides a reasonable estimate of T_g combined with estimating the T_w using meteorological observations provided an estimate of WBGT within ±2°C (at a confidence level of 95%) (Bernard and Barrow 2013).

Similar to the Bernard and Barrow (2013) study, other studies have estimated the black globe temperature and/or the natural wet bulb temperature in an attempt to estimate WBGT. Working under the USARIEM, Matthew et al. (2001) estimated the mean radiant temperature,

which is used for the solar aspect of the ARIEM heat-stress model. They were able to compute the components of the WBGT which are sensitive to solar radiation. The authors proposed methods to compute T_g and T_w for use in estimating WBGT from mean radiant temperature and other standard meteorological measurements. A physical model was created by collecting meteorological measurements (air temperature, relative humidity, wind velocity, solar radiation, etc.) recorded at weather stations. This model estimated both T_g and T_w and was found to provide a close estimate of WBGT (Gaspar and Quintela 2009). Another model created by Liljegren et al. (2008) also used meteorological measurements available at weather stations located at chemical depots throughout the United States. The model, comprised of sub-models for T_g and T_w, successfully estimated WBGT within ±1°C, which is considered an acceptable estimation.

Another study also developed empirically derived methods of calculating T_g and T_w, constructed using standard meteorological measurements collected at 15 minute intervals from the Savannah River Site (Hunter 1999). The formulas are straightforward to use, and all data are freely accessible to anybody with internet access. This method produces an overall average difference of 0.5°C between the estimated WBGT and the observed. The Hunter method of calculating WBGT has been used in studies to estimate WBGT in other locations. In Sao Paulo, Brazil, a modified version of the Hunter method was used successfully in monitoring heat stress when data is collected within a distance of less than 80km (Maia et al. 2013). Also using the Hunter method, Dimiceli et al. (2011) were able to derive their own formula to estimate T_g using readily available standard meteorological measurements provided by the National Weather Service (NWS). The only difference between it and the Hunter method was that the convective heat transfer coefficient was empirically derived on site rather than assigned a constant. The 4th

order polynomial used in the Hunter method was reduced to a linear approximation between critical values using regression analysis, yielding a simpler calculation of T_g.

The risk of heat-related illnesses and deaths is not limited to the United States. Tonouchi et al. (2006) constructed models to estimate T_g and T_w, and ultimately forecast WBGT in Japan using meteorological measurements collected from weather stations. They were able to roughly simulate WBGT, but were unable to validate and improve their method due to the lack of continuously observed data.

Estimating WBGT components carries with it some concerns. Early on, Malchaire (1976) provided detailed specifications for calculating T_w and using the wet globe thermometers, which incorporate standard meteorological measurements. Alfano et al. (2012) studied each heat flow term in the heat balance equations used to estimate $T_{w,}$ along with the effects microclimate parameters have on the multiplicity of solutions. It was found that under free convection, even the smallest difference in parameters (i.e. air temperature and mean radiant temperature) could produce multiple solutions. Thus, by the standards of ISO 7243:1989, Alfano et al. (2012) believe that if T_w cannot be directly measured, a WBGT that uses estimated components should not be used to assess heat stress. There have been problems with calculating T_g as well. It was found in one study that a large size globe will produce a higher T_g for different wind speeds, as well as radiant temperature (Juang and Lin 2007). Since wind speed was shown to be crucial in T_g and T_w, there can be errors in evaluating hot environments when T_d is greater than skin temperature.

2.3 Solar Radiation

The components of WBGT, chiefly T_g, are directly related to solar radiation. The black globe thermometer collects radiation from all sources, including direct and diffuse solar radiation along with terrestrial longwave radiation. The air temperature inside the globe increases and thus does T_g. Unfortunately, traditional WBGT devices are not used due to various problems. T_g can be estimated using solar radiation data. Traditionally, solar radiation data is collected using upward facing pyrheliometers to measure direct solar radiation, pyranometers to measure global radiation (which is both direct and diffuse solar radiation), and a shaded pyranometer to measure diffuse radiation. Longwave radiation is measured using radiometers. Smaller light sensors, approximately 5 mm in diameter, have been tested and shown to adequately measure global radiation for use in assessing hot environments (Moran et al. 2001b).

Unfortunately, the solar radiation observation network is spatially sparse. Approximately 40 stations throughout the United States directly measure solar radiation. However, methods of estimating solar radiation at observation sites throughout the United States have been constructed. Lengfeld et al. (2010) estimated solar radiation using a model that includes cloud cover data in its parameters. Observed cloud and radiation data were obtained from the Richard Assmann Observatory and the German Weather Service. It was found that parameterized solar fluxes underestimated the observations; thus, the accuracy of the estimate suffered, even after changes. Using sky cover data collected from weather stations located at Mississippi County Community Collect and the Blytheville Air Force Base, Turner and Mujahid (1984) developed a model to estimate hourly global solar radiation. The results were such that the authors believed their model fared well when compared to other cloud cover models, including the NOAA Model. Turner and Mujahid (1984) also believed that their model was less spatially limited since one of

the predictors of the hourly global solar radiation is extraterrestrial solar radiation. Another method to compute solar radiation used sky cover data collected from 47 different weather stations over a 10 year period; a parabolic curve was fitted to the data to develop a formula to estimate the percentage of clear sky solar radiation (Thompson 1976). However, the authors believe that users should be wary due to uncertainties of the observed global solar radiation and observed sky cover.

One of the other models, used by the US National Solar Radiation Database, employs estimated values of direct normal, diffuse horizontal, and global horizontal radiation to calculate the METSTAT model (Meteorological/Statistical) (Maxwell 1998). The various parameters used in METSTAT include total and opaque cloud cover, aerosol optical depth, precipitable water vapor, ozone, surface albedo, snow depth, days since last snowfall, atmospheric pressure and present weather at a location. The Northeast Regional Climate Center (NRCC) solar radiation model was based on the METSTAT model, but was updated by Belcher and DeGaetano (2007) to include cloud observations from ASOS stations equipped with ceilometers and satellite estimates of cloud layers above the maximum detection distance of ceilometers. Modifications were needed because prior to ceilometers, sky cover was estimated by trained observers. The updated NRCC model was found to have similar error in estimating the solar radiation as other models. However, this model was later replaced by one developed by Perez et al. (2002) at the State University of New York (SUNY). The SUNY model uses remotely sensed imagery from the Geostationary Observed Environmental Satellite (GOES) series to determine the amount of cloud cover. This was done by employing the inverse relationship between reflected irradiance from the atmosphere and clouds back to space and ground irradiance, which is radiation from earth's surface that passes through the atmosphere.

2.4. Land Cover and Atmospheric Response

Land-atmospheric interactions are a cornerstone of meteorological research. Throughout various locations in the United States, the land cover type can change abruptly. Developed, non-permeable urban surfaces are located next to croplands, and croplands may be next to marsh lands. How land cover affects the atmosphere is the topic of many studies and can be useful in forecasting weather and climate given the known relationships. Land cover types respond in different ways due to their various properties; the classification of land cover can be done differently as well. This impacts the way a computer model or a human forecasts for a specific area, which in turn can directly impact humans. Although methods of classifying land cover type can vary, the first step generally employs remote sensing imagery. This imagery is captured using cameras and/or sensors that record reflected or emitted energy from targets on the ground. This data capture can be done one of two ways. One method uses satellites, which incorporate sensors to capture images of the earth's surface, such as the Moderate Resolution Imaging Spectroradiometer (MODIS) device aboard the EOS AM-1 and PM-1 satellites. The other method uses aerial photography, with cameras or sensors mounted on aircrafts. Both methods can use the same technique of capturing energy responses unique to various land cover types. The energy from sunlight that strikes an object can either be absorbed, reflected, or emitted. The unique way in which a given type of land cover reflects and absorbs light is known as its spectral signature (Graham 1999). The sensors that are used often record various wavelengths of energy over the same area. These wavelengths are separated into bands, with each band corresponding to a wavelength range.

Once all of the information is collected, it is converted into useable imagery. This is done by analyzing the separate bands, identifying which land cover types are present, and assigning

them a value that corresponds to a color (i.e. identifying a water feature and assigning it to the color blue). However, classifying land cover is a relatively subjective process (Anderson et al. 1976). This subjectivity is due in part to the needs of the user. Anderson (1976) developed one of the most widely used land cover classification systems based on remote sensing information, as well as the scheme used by the United States Geological Service (USGS). The process itself, while detailed, is relatively straightforward. He defined each land cover category, which includes various types, such as residential land use being included in the urban or built-up land class.

The relationship between land cover type and atmospheric response, such as air temperature, humidity, vapor pressure, and surface/near-surface temperatures, has been of particular interest to researchers. A few of these studies have focused on the relationship between land use/land cover (LULC) and the diurnal temperature range (DTR). Through analyzing synoptic weather reports from 1980-1991, Dai et al. (1999) discovered that soil moisture, an obvious characteristic of LULC, played a secondary role in the decrease of the DTR. At the mesoscale, a warm season drop in DTR was found, which increased from the northern to the southern United States, potentially as a result of evapotranspiration from vegetation (Durre and Wallace 2001). Using a different technique, Gallo et al. (1996) collected temperature data and calculated the DTR for weather stations included in the U.S. Historical Climatology Network and compared it with LULC at 3 radii around the weather stations. It was shown that out of 10 LULC types, those that were predominantly rural showed the greatest DTR, whereas those that were predominantly urban LULC showed the smallest. These patterns were prevalent even at the extent of 10 km away from an observation site. A similar approach was used to study DTR differences due to LULC and air mass type by Scheitlin and Dixon (2010). However, 5 km grid cells were used rather than radii across a research area along part of the

Mississippi River valley. Using a three-way ANOVA test, the results showed that agricultural and urban areas had the smallest DTR, with forest types experiencing the largest DTR (Scheitlin and Dixon 2010). In the same study the authors discovered that each land type had a bimodal DTR occurring in the spring and fall, which contradicts other research citing seasonal changes in evapotranspiration as the most likely cause of the DTR trend (Durre and Wallace 2001).

Remotely sensed imagery is used to identify land surface type in the Normalized Difference Vegetation Index (NDVI), a measure of plant presence and vigor in an area. A high NDVI value corresponds to an abundance of vigorous vegetation within an area, whereas a low NDVI value corresponds to a lack of vegetation. The NDVI has been employed to explore the relationship between vegetation cover/type and meteorological observations, such as temperature. NDVI and solar zenith angle have been used to derive maximum and minimum air temperature from the surface temperature of different ecosystems in Africa; this did not return a strong relationship with change in surface temperature and air temperature (Vancutsem et al. 2010). Another study tried to determine the seasonal relationship between LULC and microclimate response using the NDVI (Stabler et al. 2005). It was determined that LULC had the largest effect on the microclimate in the summer during the early morning. It was also found that agricultural and residential land uses had the highest relative humidity, dew point temperatures, NDVI, and lowest temperature. The commercial and industrial land uses had the highest temperatures and lowest NDVI.

Urban heat islands (UHI) are phenomena in which LULC and atmospheric response is examined. The urban heat island is a relationship that describes how urban areas are warmer, particularly overnight, than the surrounding un-urbanized areas due to the materials used to develop urban areas being able to retain heat very well. The relationships between the growth of

urban areas and the climate are of interest to researchers. Rather than use NDVI, Weng et al. (2004) chose to use Landsat Enhanced Thematic Mapper Plus (ETM+) images to study the relationship between land surface temperature (LST) and UHIs. The authors unmixed the banded images because the remotely sensed data comes in various wavelengths, which correspond to different materials. This allows each type of material to be identified within the range of sensed wavelengths. The authors then determined that the LULC showed a stronger negative correlation with LST across all land cover types than NDVI. This corresponds to a more direct relationship with radiative, thermal, and moisture properties, all of which determine LST and are related to air temperature. Other studies have used similar methods of determining LULC based on the un-mixing of banded imagery and have shown that land surface temperature is positively correlated with impervious surfaces (urban LULC) and negatively correlated with vegetation-covered surfaces (Carlson and Arthur 2000; Cermak et al. 2016; Lu and Weng 2006). It was also found that vegetation plays a larger role in surface temperature variations during the day while pavement plays more of a role at night (Buyantuyev and Wu 2010).

Other methods used to assess the LULC relationship with atmospheric response include the derivation of empirical models. Using regression modeling, Heisler et al. (2016) used meteorological observations and LULC indices to map air temperature patterns between locations in downtown Baltimore, MD and other proximate locations. This could be used to estimate the effect of LULC change on climate. In other model simulations, areas in which forested land cover was converted to croplands throughout the Midwest and northeastern United States, climate model simulations produced a decrease in both maximum and minimum temperature (Bonan 2001). Maximum temperature showed the greatest change, resulting in a

decrease in the DTR. Bonan (2001) observed an overall cooling of the climate over the region; simulations showed that the cooling is greater now since the reforestation of the Northeast.

Other studies have manipulated mesoscale models which were specifically developed and used for meteorological purposes to assess how they handle variations in LULC (incorporated into said models). One such model employed is the Weather Research and Forecasting (WRF) model. This model includes both the USGS and MODIS LULC classification options, but it maintains the ability to be replaced with other classification methods, as long as specific criteria are met. Using the Advanced Research WRF (WRF-ARW), Cheng et al. (2013) replaced the usual LULC classifications with one developed at the National Central University (NCU) in Taiwan in order to remove the error in showing western Taiwan as overly urbanized. Comparing the USGS, MODIS, and NCU LULC classifications, it was found that the WRF (using the USGS classification) over-predicted surface wind speeds and under-predicted daytime temperature. MODIS over-predicted temperatures, but was in close agreement with the NCU in wind speeds. Qu et al. (2013) used the same model as Cheng et al. (2013) to analyze the impact that LULC change has on the climate in north China. However, rather than use a more localized LULC classification, the MODIS dataset available for the study area was reclassified for a test of data from 2005; Global Land Cover Classification, an older LULC dataset, was used for an analysis of data from 1992. In doing so, it was discovered that the regional urbanization (a change in LULC to urban) in North China led to an increase in near-surface temperatures.

Other remotely sensed LULC data, such as Landsat-based LULC data, was used to determine the impact of LULC changes of near-surface temperatures during extreme heat events in Phoenix, Arizona (Grossman-Clarke et al. 2010). This showed that urban expansion led to a larger area experiencing extreme temperatures, with the nighttime temperatures being more

affected than the daytime. A different version of the WRF, the Non-Hydrostatic Mesoscale Model (WRF-NMM) has been used to assess how urbanization changed the daily maximum temperature in California from 1950-1954 and 2009-2013 (Sequera et al. 2015). LULC derived from historical maps was used in lieu of available imagery for the former time period; the available LULC imagery for the latter time period was updated. Results showed that change in LULC led to a change in daily maximum temperature by more than 1°C/60 years, both along coastal/non-urban regions due to large-scale climate factors (e.g., warming of sea surface temperatures) and increased urbanization. Manipulation of other models, mainly the fifth generation Mesoscale Model (MM5) developed by Pennsylvania State University and National Center for Atmospheric Research, have shown than with an updated LULC dataset possessing different thermal properties than what is traditionally used, increased the capability to simulate both daytime portion of the diurnal temperature range and near-surface temperatures during the nighttime in the urban area (Grossman-Clarke et al. 2005).

Although the studies show that differing LULC on the mesoscale has an effect on atmospheric response, most of them do not discuss the direct impact to human health. Change in LULC can lead to a number of conditions that point to serious health hazards for humans. For example, an increase in the number of extreme heat events could lead to an increase in the number of heat-related illnesses and deaths that occur in the United States. Conversely, an increase in air temperatures in urban areas may have benefits in cooler seasons (Watkins et al. 2007), which in turn could be better for those who are homeless. Knowing how LULC impacts the environment can lead to the development of better methods to improve the lives of humans in both the rural and urban environment, especially when changes in the climate may be more extreme.

The climate throughout the United States, and subsequently Indiana will change (Pryor et al. 2014). LULC analysis may show increased urbanization. Additionally, areas may be cleared for agricultural use, which would subsequently change how the environment of that area responds. That, coupled with the increasing temperatures and rising carbon dioxide levels could increase crop yields, but may be offset by extreme weather events, including EHEs (Pryor et al. 2014). These changes in LULC, temperature, cloud cover, and other weather conditions will have a direct impact on humans who spend time outdoors. An urban environment may be hotter, and agricultural land may provide more moisture to the overlying air due to the evapotranspirative properties of the land. This is why it is important to understand how the WBGT responds to various LULCs. Although their numbers are decreasing, farm hands are affected by agricultural land types, and if air temperatures and moisture increase in the air, the WBGT is anticipated to change as well; this creates an environment in which heat-related illnesses are more likely. Construction workers located in urban areas would be affected by increasing temperatures, which may magnify the heat stress experienced, thus making for a more dangerous work environment. With such a change, an assessment of indices and measurements which correspond to the impacts the environment can have on humans must take place. Although we see how the basic measurements such as temperature and humidity change between different LULC types, how do the more complex measurements, such as WBGT, change between them? Is there a correlation, or are there other factors affecting the WBGT? That is the goal of this study, to determine if there is a correlation between the WBGT and the LULC type in the hopes of better understanding the relationship between land and atmosphere, and providing insight on how it may affect humans.

III. Data and Methodology

3.1 Study Area

The area of focus of this study is the state of Indiana. The data required for this study include meteorological variables (dry-bulb temperature, wet-bulb temperature, wind speed, and estimated globe temperature), solar data for 15 Automated Surface Observation System (ASOS) weather stations throughout Indiana and 3 weather stations in Kentucky, and LULC type for Indiana. The 18 stations found in Table 3.1 were chosen because solar data is either measured or calculated for these. There are three stations in Indiana in which solar radiation is measured or calculated, but were excluded from the study area due to their proximity to other stations; this would limit any spatial bias. The three Kentucky stations were included because the spatial analysis techniques used did not fully cover the entire state of Indiana. To compensate, the three Kentucky stations were included in order to provide adequate spatial coverage (Figure 3.1). The Kentucky stations that were chosen are along the Ohio River, which forms the border between Indiana and Kentucky. Using particular locations helped limit the inclusion of land area in Kentucky, or any other state, which could potentially compromise results when WBGT is calculated.

Table 3.1: Weather stations, International Civil Aviation Organization ID, and location of the 18 weather stations within the study area

	Weather Station	ICAO ID	Location
1	Delaware County Regional Airport	KMIE	Muncie, Indiana
2	Elkhart Municipal Airport	KEKM	Elkhart, Indiana
3	Evansville Regional Airport	KEVV	Evansville, Indiana
4	Fort Wayne International Airport	KFWA	Fort Wayne, Indiana
5	Gary/Chicago International Airport	KGYY	Gary, Indiana
6	Goshen Municipal Airport	KGSH	Goshen, Indiana
7	Huntingburg Airport	KHNB	Huntingburg, Indiana
8	Indianapolis International Airport	KIND	Indianapolis, Indiana
9	Kokomo Municipal Airport[1]	KOKK	Kokomo, Indiana
10	Purdue University Airport	KLAF	Lafayette, Indiana
11	Monroe County Airport	KBMG	Bloomington, Indiana
12	Porter County Regional Airport	KVPZ	Valparaiso, Indiana
13	Shelbyville Municipal Airport	KGEZ	Shelbyville, Indiana
14	South Bend International Airport	KSBN	South Bend, Indiana
15	Terre Haute International Airport-Hulman Field	KHUF	Terre Haute, Indiana
16	Louisville International Airport-Standiford Field	KSDF	Louisville, Kentucky
17	Cincinnati/Northern Kentucky International Airport	KCVG	Covington, Kentucky
18	Berkley Regional Airport	KPDH	Paducah, Kentucky

[1] Kokomo Municipal Airport has an Automated Weather Observing Station (AWOS) rather than an ASOS Station.

Figure 3.1: Map of study area and weather station locations. Station names can be found in Table 3.1.

3.2 Data Collection

The first step was to identify days that were relatively cloud-free throughout Indiana between May 1 and September 30 from 2005 to 2010. This date range was selected because in Indiana, May through September represents the warm season in Indiana. For a day to be considered, a majority of the stations had to meet certain criteria, which are summarized in Table 3.2. The identification was done by analyzing remotely sensed visible satellite images centered over Evansville Regional Airport, which was the only adequate source whose spatial coverage included all of Indiana, at 1800 UTC produced by the National Oceanic and Atmospheric Association's (NOAA) Aviation Weather Center (AWC), accessed through the University Corporation for Atmospheric Research's (UCAR) Image Archive Meteorological case study selection kit (Ahijevych 1999) (available at http://www2.mmm.ucar.edu/imagearchive/). Out of a total of 753 days for potential analysis, only 147 (~19.5% of total) days were judged to be good candidates. The days were analyzed further by cross-referencing the satellite images with the cloud cover reported in the raw METAR observations, which were accessed from the Iowa Environmental Mesonet (IEM) ASOS-AWOS-METAR Data Download archive (Herzmann 2001) (available at https://mesonet.agron.iastate.edu/request/download.phtml), at each station at approximately 1800 UTC. After cross-referencing, 16 days were determined to be good candidates to study further, with only three days where all 18 stations reported no cloud cover at any level of the sky.

In a technique used by Scheitlin and Dixon (2010), the 16 days were then analyzed to identify whether they were synoptically weak because "synoptic-scale forcing minimizes the influences of smaller-scale variables (such as LULC type) on temperature." Synoptically-weak days were defined as days in which 850 millibar wind speed is less than 15 knots, surface wind

speed less than 10 knots, and the same air mass is over the entire study area to make sure that cloud cover, wind speed, and atmospheric moisture are relatively consistent throughout, as defined by Sheridan (2002). Upper air soundings are not performed in Indiana, so 850 millibar maps produced by NOAA's Storm Prediction Center (SPC) and accessed through the UCAR image archive (Ahijevych 1999) (available at http://www2.mmm.ucar.edu/imagearchive/) were used to analyze wind speeds over the area. These maps are only published for 0000 UTC and 1200 UTC each day. With the time of focus being 1800 UTC and 850 millibar winds not changing drastically throughout the day while one air mass is over the area, the 1200 UTC map for each of the days was used to analyze the wind speed.

Surface wind speed, dry-bulb temperature, and wet-bulb temperature for each station were collected from NOAA's Quality Controlled Local Climatological Data (QCLCD) archive provided by the National Center for Environmental Information (NCEI) at approximately 1800 UTC (available at https://www.ncdc.noaa.gov/qclcd/QCLCD?prior=N). For any stations in which data were missing for those three days in the QCLCD dataset, the appropriate variables were obtained through NOAA's National Data Center (NNDC) (Baldwin) (available at https://www7.ncdc.noaa.gov/CDO/cdoselect.cmd?datasetabbv=GSOD&countryabbv=&georegionabbv). To determine whether or not the air mass over Indiana is the same, the air mass data was obtained from the Spatial Synoptic Classification (SSC) (Sheridan 2002) (available at http://sheridan.geog.kent.edu/ssc.html). There are four stations in Indiana that are included within the SSC network: Evansville, Fort Wayne, Indianapolis, and South Bend. Each day, the dominant air mass over the area is classified by one of the following SSCs: DP (dry polar), DM (dry moderate), DT (dry tropical), MP (moist polar), MM (moist moderate), and MT (moist tropical) which also includes MT+ (moist tropical plus) and MT++ (moist tropical double plus).

The explanation of each air mass is described by Sheridan (2002). In order to minimize the effect of latitudinal changes in temperatures, air masses over the area need only be of similar moisture since WBGT is so reliant upon wet-bulb temperature (T_w). After the analysis, it was determined that July 19, 2006, August 28, 2007, and September 3, 2007 were suitable days for this study with September 3, 2007 being the only day in which there were no clouds reported at any of the 18 stations.

Table 3.2: Criteria for days to be considered for analysis

Criteria
- Station Temperature ≥ 30°C
- Station reporting "clear" or "few" for sky cover
- ≤ 15 knot 850 mb wind speed
- ≤ 10 knot surface wind speed
- Air masses over area having same moisture characteristic

For each of the 18 stations, the WBGT was calculated for each of the three days using the following equation by Yaglou and Minard (1957):

$$WBGT = 0.7*T_w + 0.2*T_g + 0.1*T_d \quad \textbf{(eq. 1)}$$

where T_w is wet-bulb temperature, T_g is black-globe temperature, and T_d is dry-bulb temperature. T_d and T_w were collected with the wind speed from the NCEI's QCLCD archive. T_g is not directly measured at any stations in Indiana due to factors noted previously, so it must be estimated. For this study, the following equation developed by Hunter (1999) was used to calculate the black-globe temperature:

$$\begin{aligned}\left(1-\alpha_{sps}\right)S(f_{db}s_{sp}+(1+\alpha_{es})\left(f_{dif}\right)+\varepsilon_a\left(1-\alpha_{spl}\right)\sigma T_a^4 \\ =\ \varepsilon_g\sigma T_g^4+0.115u^{0.58}(T_g-T_a)\end{aligned} \quad \textbf{(eq. 2)}$$

where α_{sps} is the globe albedo for shortwave radiation (equal to 0.05), S is the total downwelling solar radiation (W/m^2), f_{db} is the fraction of direct beam solar radiation, s_{sp} is a sphere shape factor for the black-globe thermometer (equal to $\frac{1}{4\cos(z)}$), z is equal to the zenith angle, α_{es} is the surface albedo, f_{dif} is the fraction of diffuse solar radiation, ε_a is the atmospheric emissivity, α_{spl} is the globe albedo or longwave radiation (equal to 0.05), σ is the Stefan-Boltzmann constant, T_a is the air temperature (Celsius), ε_g is the globe thermal emissivity (equal to 0.95), T_g is the black-globe temperature (Celsius), u is the wind speed (in meters per hour). The variables in equation 2 were used to find T_g.[2] The atmospheric emissivity term ε_a is dependent on atmospheric vapor pressure. In the case where winds were 0 mph (0 meters per hour), the wind value was changed to 3 mph (4828.02 meters per hour), which was the next lowest wind speed value for all days, because the estimated T_g *when* $u = 0$ was not feasible. The formula used to calculate atmospheric emissivity (ε_a) is as follows

$$\varepsilon_a = 0.575 e_a^{1/7} \quad \textbf{(eq. 3)}$$

where e_a is atmospheric vapor pressure, which is calculated by

$$e_a = \exp\left(\frac{17.67\left(T_{dp} - T_d\right)}{T_{dp} + 243.5}\right) * (1.0007 + 0.00000346P) * 6.112 \exp\left(\frac{17.502 T_d}{240.97 + T_d}\right) \quad \textbf{(eq. 4)}$$

where T_{dp} is dew point (°C) and P is barometric pressure (mb). Equation 2 was used rather than that of Dimiceli et al. (2011) because of the convective heat transfer coefficient term (h) that is

[2] The variables for equation 2 can be found in Appendix A

used for each. Hunter (1999) assigns *h* a constant value of 0.115 in his equation, whereas Dimiceli et al. (2011) empirically derived *h* to be

$$h = a\,(S^b)\,[\cos z]^c \qquad \textbf{(eq. 5)}$$

where *S* and *z* are noted in equation 2, and the variables *a*, *b*, and *c* were determined using multiple power regression. Empirically deriving *h* reduces equation 2 to a simple linear equation and thus becomes easier to solve. However, using Hunter's *h* allows for the data to refrain from consistently going through multiple power regression before use. One caveat is that the determination of his value for *h* is not explained, so how he arrived at it is not well understood.

The solar data needed for equation 2 was obtained from the National Renewable Energy Laboratory's (NREL) 1991-2010 National Solar Research Database (NSRDB) (Wilcox 2012) (available at http://rredc.nrel.gov/solar/old_data/nsrdb/.) The database provides three classes of data according to the NSRDB User Manual. These are:

- "Class I stations have a complete record (all hours 1991-2010) for solar and key meteorological fields and have the highest quality solar modeled data (242 sites).
- Class II have a complete period of record, but significant periods of interpolated, filled, or otherwise lower-quality input for the solar models (618 sites).
- Class III has some gaps in the period of records, but has at least 3 years of data that might be useful for some applications (594 sites)" (Wilcox 2012).

The number of classes for the stations can be seen in Table 3.3. Although no stations throughout Indiana measure solar data directly, the NSRDB User Manual provides a chart, similar to that of Figure 3.2, which provides information of the quality of the data provided. All stations throughout Indiana and Kentucky have high data quality for the years of 2006 and 2007 despite the lack of direct measurements.

Table 3.3: Number of stations in the study area which fall under each of the NSRDB classes.

NSRDB Class	Number of

	Stations
Class I	7
Class II	4
Class III	7

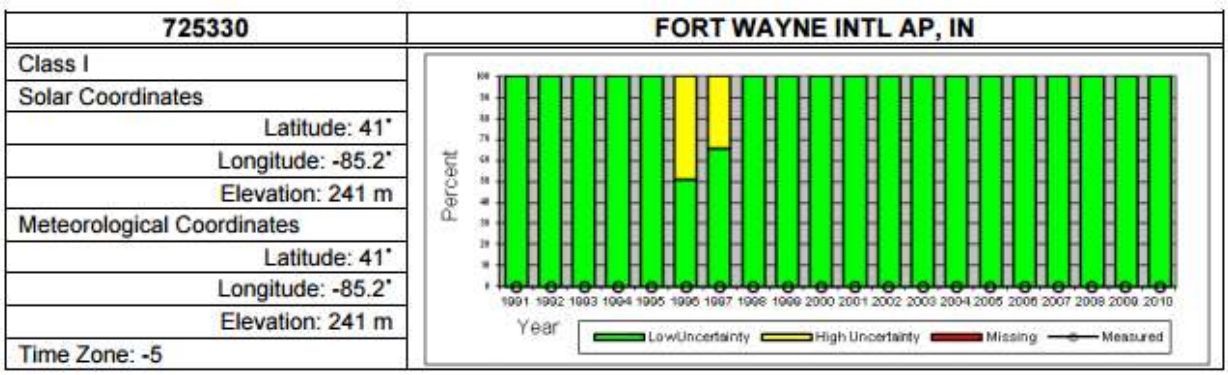

Figure 3.2: Example of station location information within the NSRDB, with the bars on the right showing percentage of uncertainty of the data, along with percent of measured data.

The NSRDB does not have access to any stations in Indiana that measure solar radiation directly. To remedy this, their database includes two models, the SUNY model and the METSTAT model (Meteorological/Statistical). The way the model determines the cloud cover is by using the inverse relationship between radiation that is reflected by the atmosphere and cloud back to space (reflected irradiance), and radiation that is transmitted to the earth's surface through the atmosphere (ground irradiance). The METSTAT model uses cloud cover data from the ASOS stations as well as ASOS Supplemental Cloud Product developed by Graumann (2003), which uses remotely sensed satellite images for estimated total cloud cover; this method also incorporates cloud height information. Both of these models have uncertainty associated with them, but the SUNY data uncertainty is much less than the METSTAT, so the SUNY model data was used.

3.3 Data Analysis

Multiple different methods of data analysis were used to determine if there exists a relationship between LULC and WBGT, as well as methods similar, but not the same as those used by Scheitlin and Dixon (2010). Some variables were changed for use in this study, one of which is the surface albedo (α_{es}). The surface albedo is provided in the solar radiation dataset for each station. However, the focus is not the stations themselves, but rather the land cover throughout the entire state. The surface albedo used for each land cover category reflects values that are the mean of a range of surface albedo values at the station location provided by Oke (1987). The other data is the amount of solar radiation. The NSRDB does not provide estimated total solar radiation (*S*). Rather, it provides global horizontal irradiance (GHI), the amount of solar radiation received at a surface horizontal to the surface, which is a portion of S. Also included is direct beam solar radiation (*db*) and diffuse solar radiation (*dif*). So, *S* is the sum of *db* and *df*. The units in equation 2 for *S*, f_{db}, f_{dif} are W/m^2 (Watt per meter squared) whereas the units for solar radiation provided by the NSRDB data is Wh/m^2 (Watt-hour per meter squared), which is the amount of solar radiation during the previous hour, ending at the reported time. The NSRDB units are used for the purpose of this research as instantaneous information on solar radiation amount is not feasible for any of the 18 stations and since it is likely that unless conditions drastically changed within an hour, the fraction of direct beam and diffuse radiation at any instance is similar to that collected over an hour. Once all of the appropriate solar radiation data was gathered, equation 2 was solved in Microsoft Excel. However, this produces a 4th order polynomial of the general form

$$ax^4+dx-c = 0 \quad \textbf{(eq. 6)}$$

which is not easily solved. So, using an Excel macro accessed from excelcalcs.com and produced by Tomanovich (2008), equation 4 was solved for *x* (in this case $x = T_g$) using the Jenkins-Traub

method. This method is designed to solve special case polynomials with real coefficients. As with solving polynomials of any order greater than 1, multiple solutions were produced. In this case, four real solutions and two imaginary solutions were produced. The actual solution in each case was obvious as the imaginary solutions were not mathematically possible, and the other three real solutions were not in the range of possible solutions.

The geographic location of the stations within Indiana and Kentucky can be seen in Figure 3.1. Tiger/line shapefiles of Indiana and Kentucky were obtained from the United States Census Bureau Data Catalog (Census 2014) (available at https://www.census.gov/geo/maps-data/data/tiger-line.html.) The National Land Cover Dataset for 2006 for Indiana was obtained from the USGS Land Cover Institute (Fry et al. 2011) (available at https://landcover.usgs.gov/landcoverdata.php.) The LULC data from the USGS is based on Landsat Thematic Mapper data from the Multi-Resolution Land Cover Consortium (MRLC), which identifies LULC in 30 meter grid cells. Each LULC is given a corresponding value based on rules established by Anderson et al. (1976). Although some types of LULC in the new categories have different characteristics, for example developed, open space being very different from developed, high intensity, the new classification system used for this study used the same scheme as the NLCD classification scheme due to the unknown qualitative differences between the LULC types within the resampled classes. The land cover was constrained to the extent of the Indiana state border using the Clip tool in ArcGIS. (Figure 3.3).

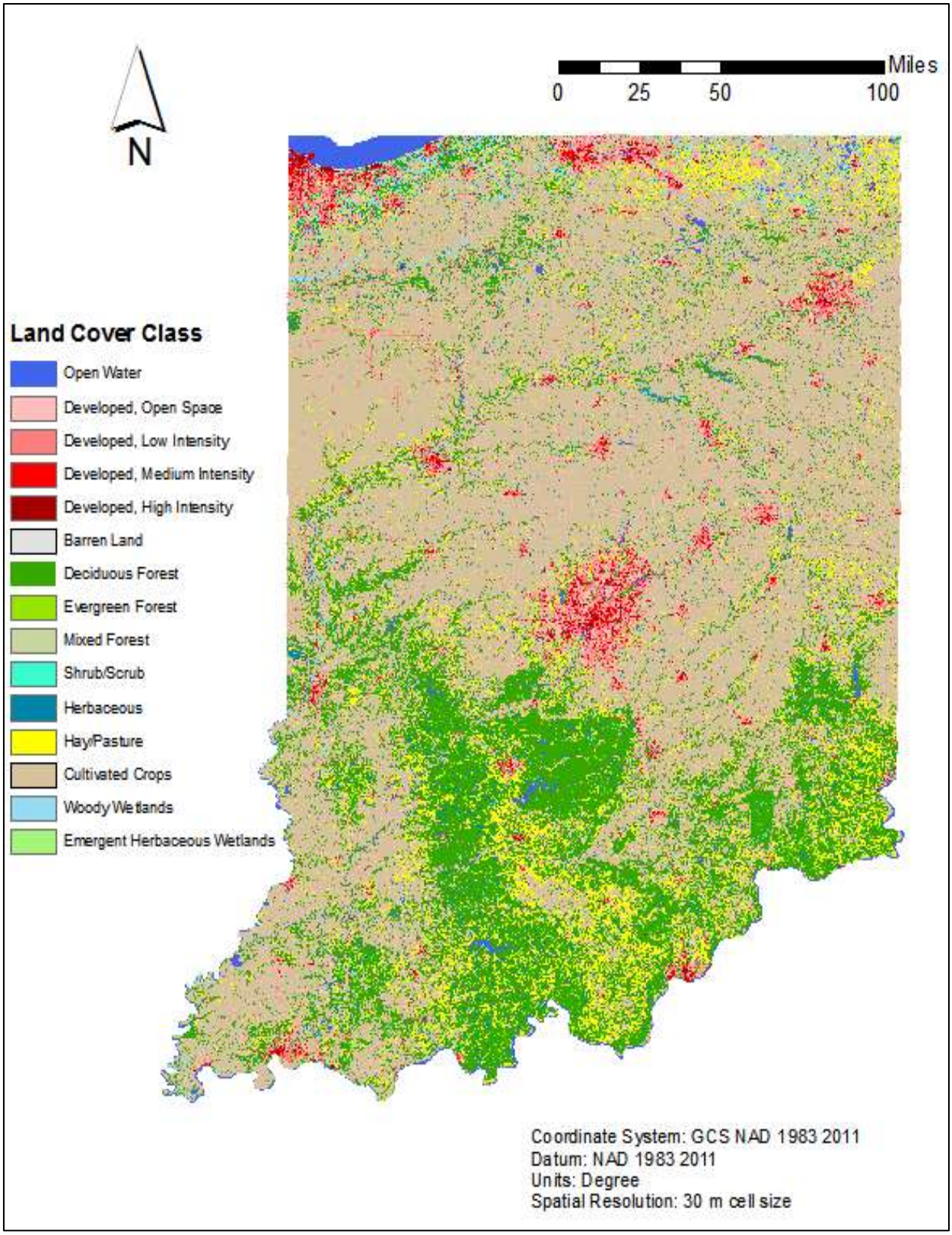

Figure 1.3: LULC map of Indiana using USGS 2006 National Land Cover Dataset

The 30 meter LULC data was reclassified into 7 groups rather than keeping the original 14 groups. This was done because, although each LULC is unique, some possess similar properties. So, similar LULC types were grouped together (Table 3.4). Using a technique based on one used by Scheitlin and Dixon (2010), the land cover was resampled to 5 km grid cells (Figure 3.4). In order to analyze this data, the resampled LULC raster layer was converted to a shapefile where each cell is its own polygon. This was done by resampling the 30 meter LULC raster layer into 5 km grid cells. The 5 km grid cells were used because it is believed that small sections of LULC do not have a significant effect on climate (Scheitlin and Dixon 2010). So, the larger scale has more of an effect on the heat stress experienced by humans, despite the heat stress on humans being experienced at a smaller scale. This new raster layer was then converted to a polygon shapefile and the 5 km polygon shapefile was clipped to the extent of the Indiana shapefile. Each polygon was then assigned the most common cell value from the NLCD 2011 raster layer. The attribute tables were joined and a field was created to calculate the land cover code (Table 3.4).

Table 3.3: Original and reclassified Land Cover Classes and Assigned Code

Original Land Cover Classes		Reclassified Land Cover Classes	
1	Woody Wetlands	1	Woody Wetlands/Emergent Herbaceous Wetlands
2	Shrub/Scrub	2	Shrub/Scrub/Herbaceous/Hay/Pasture
3	Open Water	3	Open Water
4	Mixed Forest	4	Deciduous Forest/Evergreen Forest/Mixed Forest
5	Herbaceous	5	Developed
6	Hay/Pasture	6	Cultivated Crops
7	Evergreen Forest	7	Barren Land
8	Emerging Herbaceous Wetlands		
9	Developed, Open Space		
10	Developed, Low Intensity		
11	Developed, Medium Intensity		
12	Developed, High Intensity		
13	Deciduous Forest		
14	Cultivated Crops		
15	Barren Land		

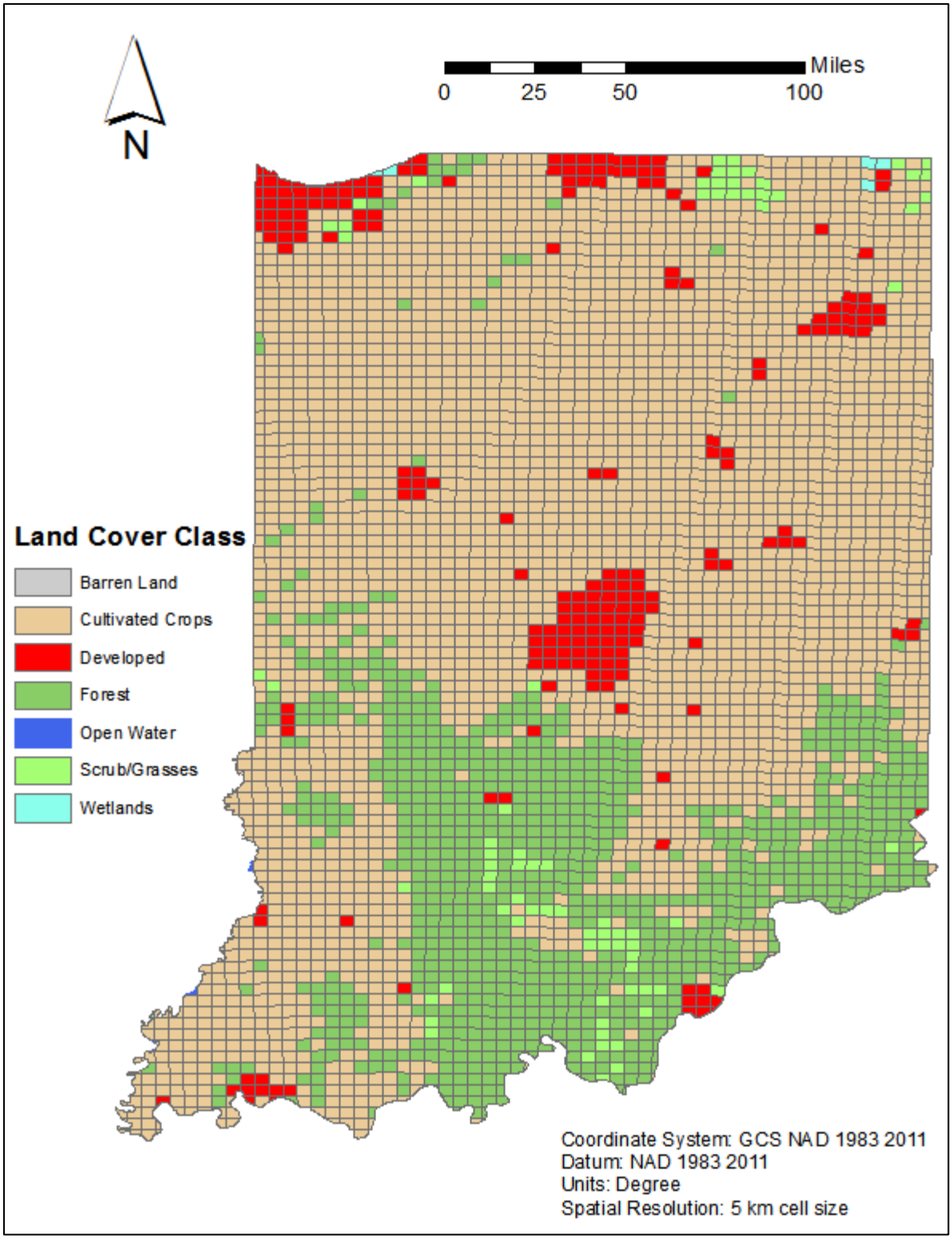

Figure 3.2: Reclassified and resampled 5 km LULC map of Indiana using USGS 2011 National Land Cover Dataset

The station information for each of the weather stations in the ArcGIS point shapefile did not include the estimated WBGT, which had to be entered manually for each of the three days. Three raster layers, one for each day, were then created using the inverse distance weighted interpolation tool in ArcGIS in order to show the spatial variation of the estimated WBGT throughout Indiana (Figures 3.5-3.7). This tool used the nearest five points to each individual location and assigned each a weight. The 5 km polygons were then assigned a mean WBGT using the Zonal Statistics as Table method, but with "mean" as the statistics type. This allowed each cell to have both a WBGT value and a land cover code. Of the 3901 total grid cells, 77 were excluded from the study area because they were either 1.) too areally small for use with zonal statistics and WBGT calculation because the produced a value close to zero or 2.) the raster did not completely cover an entire cell. The excluded cells were all along the state boundaries.

To determine whether LULC and estimated WBGT were related, a Kruskal-Wallis test was conducted using SPSS (IBM). The Kruskal-Wallis test determines the probability of making a type I error when rejecting the null hypothesis, which states that the estimated WBGT for the compared LULC classes are drawn from the same population, and therefore not significantly different. If it is determined that the samples are drawn from the same population (i.e., accept the null hypothesis), it is reasonable to believe that the LULC type does not affect the estimated WBGT. However, the Kruskal-Wallis test only shows that there is a significant difference in the estimated WBGT for each LULC class, not which classes are significantly different from each other. That required the use of Dunn's post-hoc analysis in order to determine which LULC type's estimated WBGT distribution is significantly different from the others. Dunn's post-hoc analysis returned an adjusted significance value. The significance is adjusted by the Bonferroni correction due to the compounding of the significance level when running multiple tests. A

random number generator in Excel was used to provide the first sample cell. A systematic sample of 294 grid cells was taken out of the total number of cells (3818) based on their unique identifiers. This was done by sampling every 13th cell after the first was determined. This was done because adjacent cells are spatially dependent upon one another, meaning LULC type and WBGT for cells that are adjacent to each other are going to influence one another. This spatial dependency would affect the WBGT in adjacent cells. In order to limit that, a systematic sample was take so that cells were non-adjacent. However, due to the geographic shape of Indiana, especially southern Indiana, systematically selecting non-adjacent cells was impossible. There were a limited number of adjacent cells. The breakdown of the number of cells for each LULC class throughout Indiana can be found in Table 3.5.

Table 3.4: Number of cells in each Land Cover Class.

Land Cover Class	Count
Barren Land	1
Cultivated Crops	2625
Developed	221
Forest	882
Open Water	3
Scrub/Grasses	80
Wetlands	6
Total	3818

Although there was a limited number of adjacent cells included within the sample, it is believed that they will have a small overall impact on the results. This is due to most of the adjacent cells having the same LULC type and a close enough estimated WBGT to not be significantly different, i.e. being spatially dependent. However, the small number of Scrub/Grasses LULC cells may result in a small number of those being sampled, and thus an inconclusive result when comparing the Scrub/Grasses LULC cells with others. However, since

the sample sizes of the Scrub/Grasses class were so small, these samples were discarded, and the Kruskal-Wallis test and Dunn's post-hoc analysis were re-computed. Although this produced different sample sizes for each day, they were not so different that it greatly affected the results.

Regardless of the factors that could impact the estimated WBGT, the methods used to determine whether a relationship exists between the estimated LULC type and estimated WBGT were valid. Other methods of estimating the WBGT would require resources not available and collecting primary data is too time consuming. Multiple studies have either used the method of WBGT estimation developed by Hunter (1999), which was determined to be accurate within 0.5° C or they made slight modifications to the equation for their own research (Dimiceli et al. 2011; Maia et al. 2013). While that difference in accuracy may make a difference in the use of the WBGT in real-world scenarios, for the purpose of this study, the method of calculating the WBGT is as accurate as possible without knowing what the results of primary data collection would yield.[3]

[3] A flow chart for the methodology can be found in appendix B

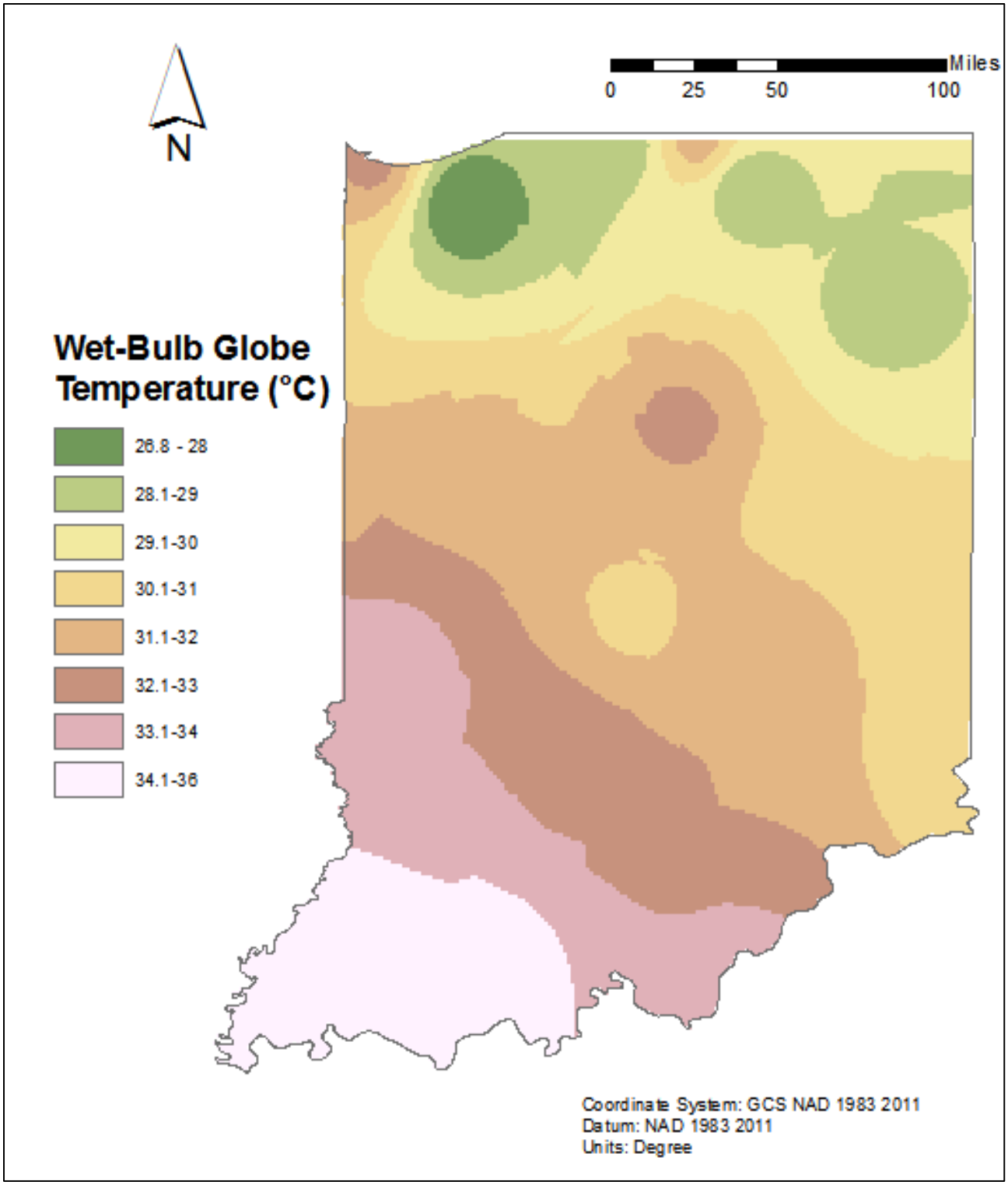

Figure 3.3: Estimated Wet-Bulb Globe Temperature raster layer for July 19, 2006

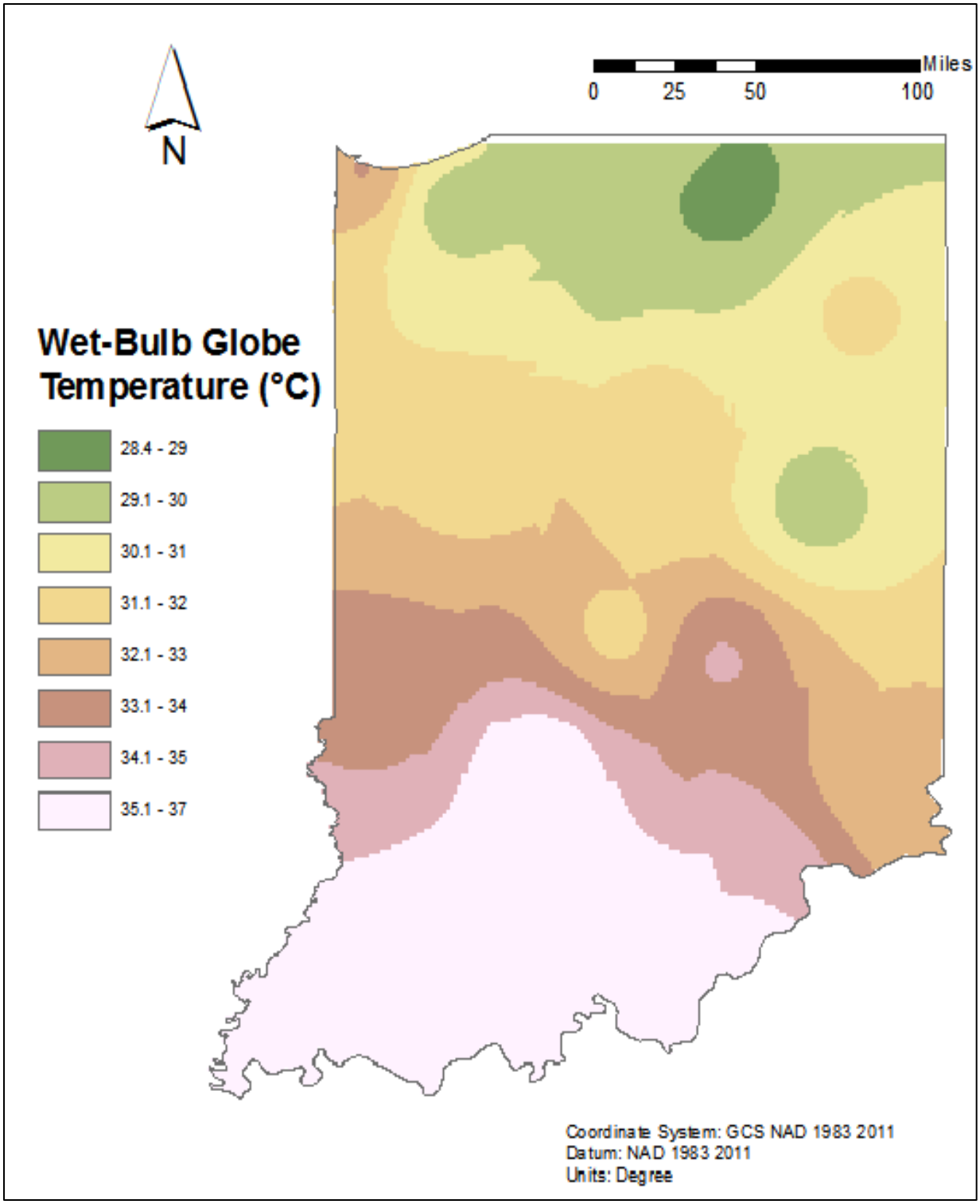

Figure 3.4: Estimated Wet-Bulb Glove Temperature raster layer for August 28, 2007

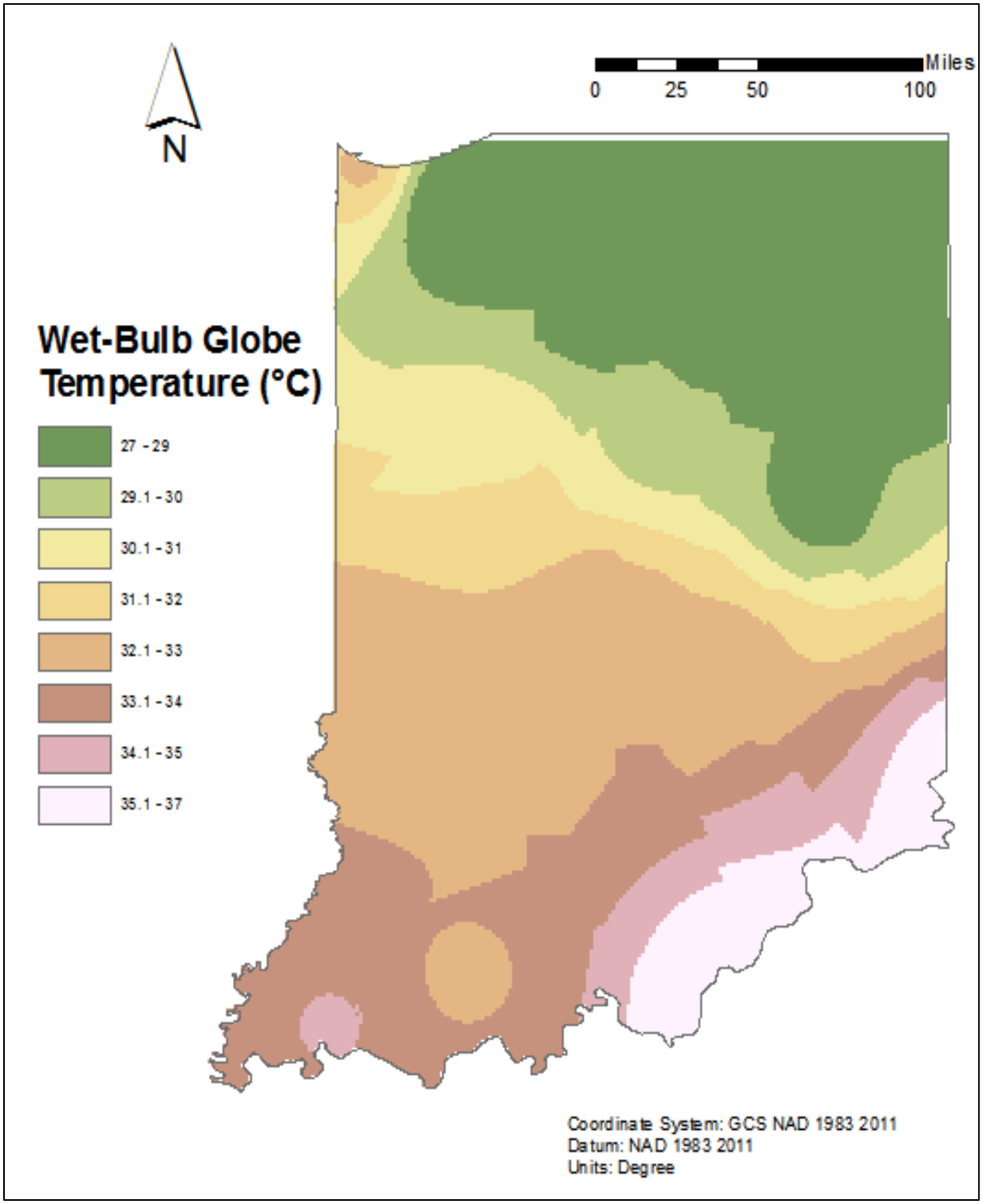

Figure 3.5: Estimated Wet-Bulb Glove Temperature raster layer for September 3, 2007

IV. Results and Discussion

Each LULC class seemed to have a wide range of WBGTs, as seen by the top and bottom of the ranges of the boxplots in Figures 4.1-4.3. For two of the three days in which samples were taken (July 19, 2006 & September 3, 2007), the Forest class recorded the highest estimated WBGT (35.33°C and 36.54°C respectively) (look at the top of the range) and the highest mean estimated WBGT (32.82°C and 33.30°C respectively). On each of the three days, the Scrub/Grasses class had either the second highest or the highest mean estimated WBGT. However, one reason why the mean-estimated WBGT of the Scrub/Grasses class may be due to the small number of Scrub/Grasses cells that appeared in each sample. The number of cells sampled in each LULC class for each day can be found in Table 4.1. For each of the three days, the Forest class also showed the smallest standard deviations, followed by Developed, Cultivated Crops, and Scrub/Grasses classes. This shows that the Forest class estimated WBGTs are closer to the mean and thus closer to the expected value. However, the mean and the standard deviation do not show the entirety of the relationship between LULC type and estimated WBGT. The results of the Kruskal-Wallis test and Dunn's post-hoc analysis is the key to establishing a relationship between LULC type and WBGT.

Table 4.1: Number of cells sampled (n) for each LULC class from the three days studied.

Class name	July 19, 2006	August 28, 2007	September 3, 2007
Scrub/Grasses	10	6	3
Forest	74	69	65
Developed	18	21	16
Cultivated Crops	192	198	210
Total	294	294	294

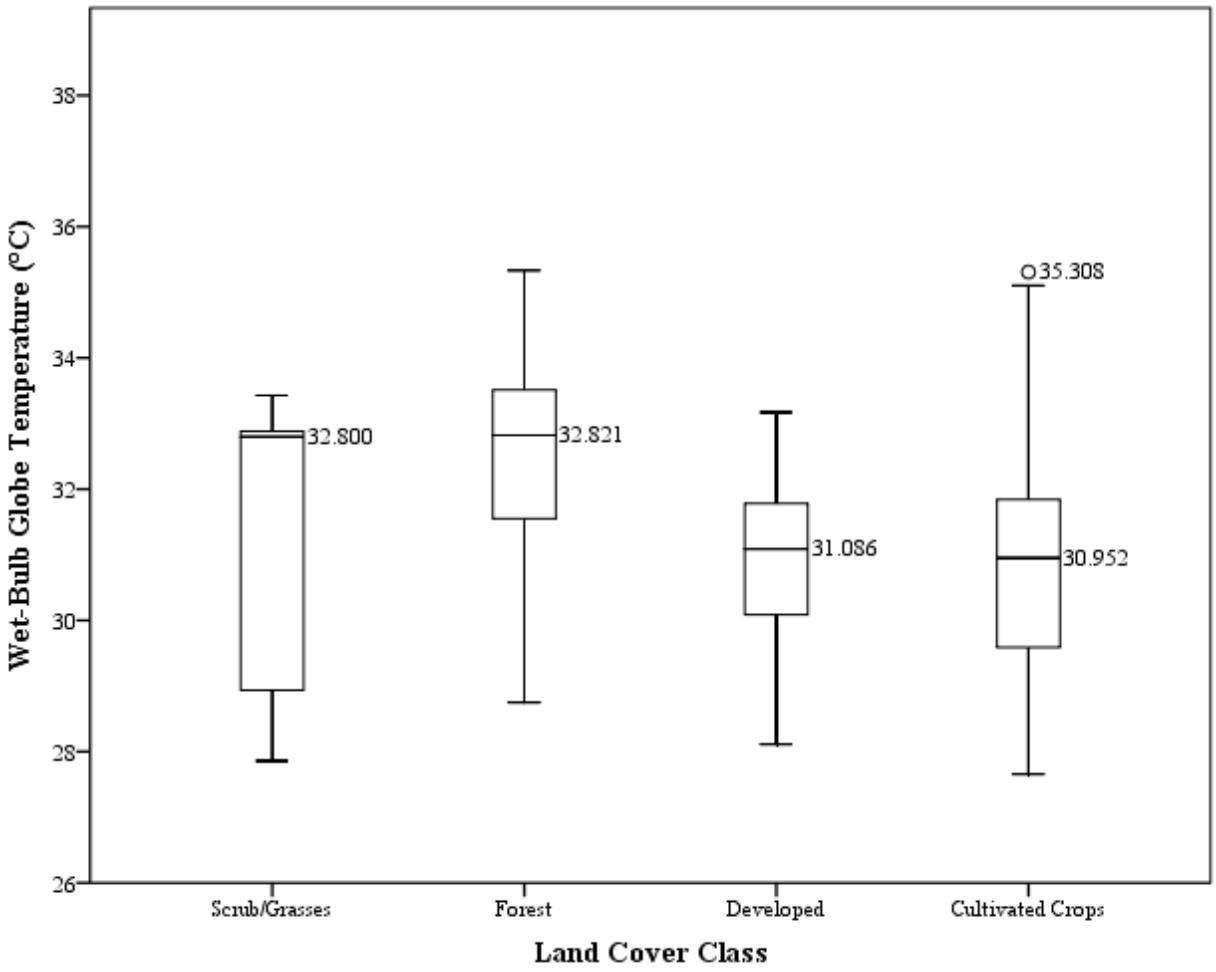

Figure 4.1: Boxplot of the Wet-Bulb Globe Temperature for each LULC class for July 19, 2006

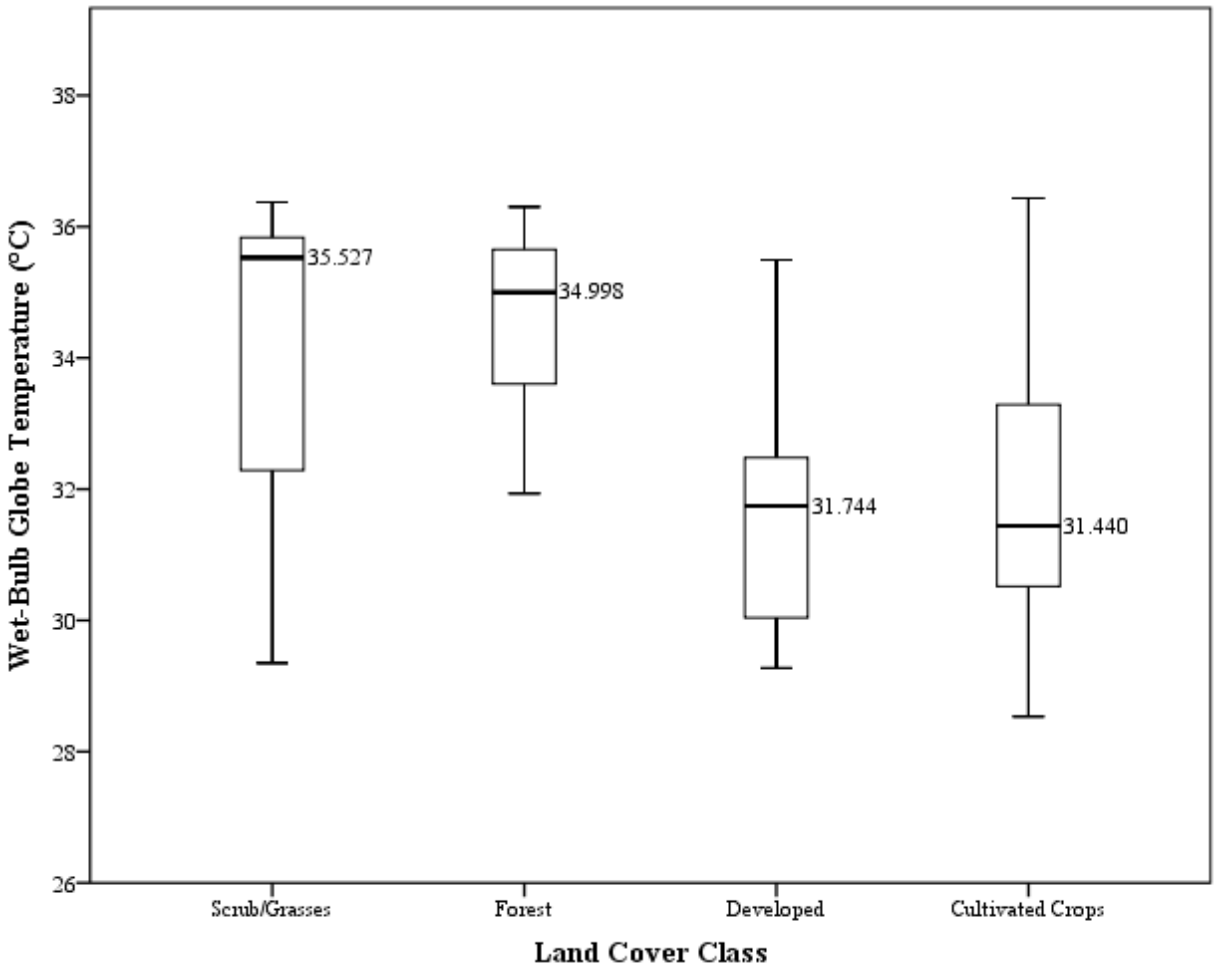

Figure 4.2: Boxplot of the Wet-Bulb Globe Temperature for each LULC class for August 28, 2007

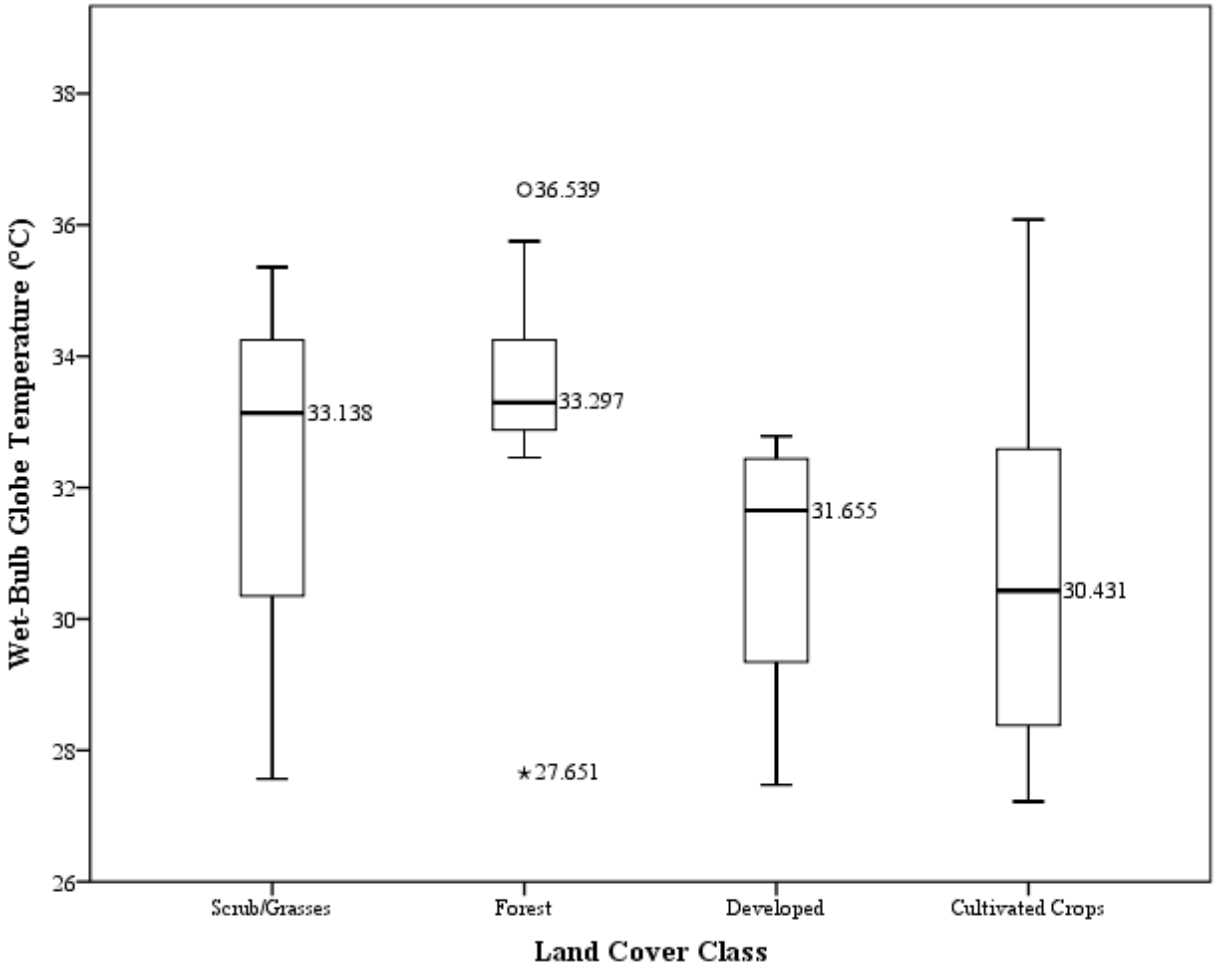

Figure 4.3: Boxplot of the Wet-Bulb Globe Temperature for each LULC class for September 3, 2007. The circle represents an outlier and the star represents an extreme outlier

For each of the three days in this study, the result of the Kruskal-Wallis test indicated a significant difference in the distribution of the samples for each day when $p \leq 0.05$ (Table 4.2), i.e., that the estimated WBGT varied by LULC types. The results of the Dunn's post-hoc analysis showed that for each of the three days, the estimated WBGT distribution of the Forest class is significantly different from the estimated WBGT distribution of the Developed and the Cultivated Crops classes ($p \leq 0.05$) (Table 4.3). The test statistics for the Dunn's post-hoc analysis in Table 4.3 is the adjusted significance. Overall, these results suggest that LULC type does play a role in the variation of estimated WBGT.

Table 4.2: Kruskal-Wallis test results for each of three days studied.

	July 19, 2006	August 28, 2007	September 3, 2007
Total N	294	294	294
Test Statistics (H)	42.453	86.353	83.703
Degrees of Freedom	3	3	3
Asymptotic Significance (p-value) (2-sided test)	0.000	0.000	0.000

Table 4.3: Dunn's post-hoc analysis results showing adjusted significance after standardizing the test statistic for comparison of each LULC class. The highlighted cells are those below $p \leq 0.05$.

Class Pairs	July 19, 2006	August 28, 2007	September 3, 2007
Developed - Cultivated Crops	1.000	1.000	1.000
Developed - Scrub/Grasses	1.000	0.081	1.000
Developed - Forest	0.003	0.000	0.000
Cultivated Crops - Scrub/Grasses	1.000	0.081	1.000
Cultivated Crops - Forest	0.000	0.000	0.000
Scrub/Grasses - Forest	0.258	1.000	1.000

Even though the results show that LULC type is a factor in the estimated WBGT, the Scrub/Grasses class was sampled at a small number. There appeared to be no significant difference in the distribution of the estimated WBGT between it and the other LULC classes when Dunn's pot-hoc analysis was performed; this can be seen in the sample taken from August 28, 2007 (Table 4.3). The standardized test statistic is performed automatically by SPSS for each LULC class, so the significance levels are adjusted to be able to compare each LULC class with one another. The comparisons between the Developed and Scrub/Grass classes and the Cultivated Crops and Scrub/Grass classes resulted in a low probability of making a type I error (if the null hypothesis is rejected). However, this low probability is not enough to meet the threshold of $p < 0.05$ for rejection of the null hypothesis. This is somewhat apparent from the comparison of the Scrub/Grasses and the Forest classes for July 19, 2006. It is believed that if the sample size of the Scrub/Grasses LULC was large enough, that there would exist a significant difference in estimated WBGT between the Scrub/Grasses class and the other LULC classes.

The results of the Kruskal-Wallis test performed with the exclusion of the Scrub/Grasses class type again show a significant difference in the estimated WBGT between the classes for each day when $p = 0.05$ (Table 4.4). The results of Dunn's post-hoc analysis again showed that the estimated WBGT distribution of the Forest class is significantly different than that of Developed and from Cultivated Crops classes at $p \leq 0.05$, but still no difference when comparing the Developed and Cultivated Crops class to each other (Table 4.5). The combination of these results help draw the same conclusion as the above analysis that included the Grasses/Scrub class, i.e., that LULC type, in some way, influences estimated WBGT.

Table 4.4: Kruskal-Wallis test results for each of three days studied with the Scrub/Grasses LULC class excluded

	July 19, 2006	August 28, 2007	September 3, 2007
Total N	284	288	291
Test Statistics (H)	43.033	84.502	84.246
Degrees of Freedom	2	2	2
Asymptotic Significance (2-sided test)	0.000	0.000	0.000

Table 4.5: Dunn's post-hoc analysis results showing adjusted significance after standardizing the test statistic for comparison of each LULC class with the Scrub/Grasses LULC Class excluded. The highlighted cells are those below $p \leq 0.05$.

Class Pairs	July 19, 2006	August 28, 2007	September 3, 2007
Developed-Cultivated Crops	1.000	1.000	1.000
Developed-Forest	0.002	0.000	0.000
Cultivated Crops-Forest	0.000	0.000	0.000

Although there does appear to be a relationship between LULC and estimated WBGT, which was expected, some of the results yielded unanticipated findings. For example, that developed areas have higher temperatures than other LULC classes is well documented, with the effect being more pronounced during the night, but still somewhat evident during the day. This is known as the urban heat island effect. However, in the study the Developed class had neither the highest overall nor mean estimated WBGT, which was unexpected. One explanation may be from latitudinal changes in dry-bulb temperature. Southern Indiana experienced higher estimated WBGTs than the northern area. Southern Indiana also is largely forested as well. So the samples taken from the forested areas may have a higher estimated WBGT because of latitude rather than variations due to other factors.

There may also be a problem with the method in which the estimated WBGT was interpolated across the state. The way ArcGIS interpolates data to form a raster is based on the number of nearest points to use for weighting. In this study, the five nearest locations were used to determine the interpolated estimated WBGT. Most noticeably seen in Figure 3.6, this creates the appearance of rings directly around some of the stations with an abrupt delineation with the adjoining WBGT ranges. Since the data network selected was so sparse (only 18 stations were taken into consideration), it created an estimated WBGT raster layer that may not be totally representative of what the actual WBGT would be at any specific location during the three days sampled.

Another factor that affected the estimated WBGT is the wind speed. The estimated black-globe temperature was drastically impacted by a change in wind speed. Any increase in wind speed would decrease the black-globe temperature, but the observed changes were greater than anticipated. Having to convert wind speed from miles per hour to meters per hour made a one mile per hour difference from station to station seem much larger, in the range of 2000-3000 meters per hour difference. A one mile per hour difference in wind speed is minor, but when converted to meters per hour the difference suddenly becomes very drastic. Such a drastic change is likely the result of the wind speed not be measured at a precise enough level in miles per hour. These large differences in wind speed, after conversion, resulted in 10°C change in the black-globe temperature in some cases. This seemingly large difference in converted wind speed likely does not have such a drastic effect on the actual black-globe temperature. The black-globe temperature itself impacted the overall WBGT more than anticipated as well, so the estimated WBGT were higher than expected. Overall, any small change in wind speed results in a greater than expected change in WBGT. However, these changes in black-globe temperature impacted

every LULC class, so the spatial pattern of the estimated WBGT is still likely to be impacted by the land cover.

V. Summary and Conclusions

A number of different studies discussed the relationship between temperature, wind speed, solar radiation, or other atmospheric variables with that of some physical feature such as land cover type. However, very few studies have discussed how heat-stress indices, such as the Wet-Bulb Globe Temperature are related to those same physical features. Those studies that do examine WBGT have the focus of determining the safety of an indoor work space, such as an aluminum smelter or steel mill. However, WBGT is used in other industries which include outdoor work spaces. The goal of this study was to determine whether LULC type was related to estimated WBGT in Indiana

Eighteen locations were used to produce maps for three different days using ArcGIS. The maps included 15 stations from Indiana and three from sites along the Ohio River in Kentucky to provide adequate spatial coverage of Indiana and to limit the inclusion of area outside the study area. Each location had an estimated WBGT assigned to it after calculation of the estimated globe temperature in Microsoft Excel. Using inverse distance weighted interpolation, WBGT maps were generated for the entire state of Indiana using ArcGIS. LULC maps were resampled from 30 m resolution to 5 km resolution. Each new cell was assigned a WBGT and a LULC code.

A Kruskal-Wallis test was performed to test whether the samples are drawn from the same population. Results indicated a significant difference between the estimated WBGT for each LULC class, meaning that LULC type likely has an effect on the estimated WBGT. Dunn's post-hoc analysis showed WBGT in the Forest class differed from both the Developed class and the Cultivated Crops class. The Forest class also exhibited the highest mean estimate WBGT on two of the three days analyzed and was a closed second highest on the third day. This may be

due more evapotranspiration, and thus more atmospheric moisture over forest regions than the other LULC classes. A second, and more likely reason, is that much of the forested region exists in Southern Indiana, where dry-bulb and wet-bulb temperatures will be greater due to latitude.

Regardless, it's believed there still exists a relationship between estimated WBGT and LULC type since the relationships between LULC type and the components of WBGT (dry-bulb temperature, wet-bulb temperature, and wind speed) are well studied. Other relationships may have existed as well if the sample size of the Scrub/Grass LULC class was large enough. Having a limited population size significantly reduced the sample size of that class.

From these results, the observed relationship between estimated WBGT and LULC type could potentially impact how we think of safety during extreme heat events. These results could lay the ground work for further research on the micro-scale, as it is becoming increasingly important to know how the weather will impact humans at finer scales. Future studies should consider different study areas, perhaps those with an already established network of weather observation sites. They should also consider the fact that many locations throughout the US do not measure the amount of radiation reaching the surface, yet measuring radiation could provide a more precise WBGT, and thus, a more precise analysis of the relationship. This information could also be extended further into how the use of synthetic surfaces in different applications will result in microclimatological changes. Knowing, for example, how migrant farmers who hand-pick crops are affected by the crop land as well as how the average person in a large urban area are affected during the same extreme heat event could literally be the difference between life and death.

Appendix A

Estimated Globe Temperature

$$\left(1-\alpha_{sps}\right)S(f_{db}s_{sp}+(1+\alpha_{es})f_{dif})+\varepsilon_a\left(1-\alpha_{spl}\right)\sigma T_a^4 = \varepsilon_g\sigma T_g^4+0.115u^{0.58}(T_g-T_a)$$

α_{sps}: globe albedo for shortwave radiation = 0.05
S: total downwelling solar radiation **(**W/m^2)
f_{db}: fraction of direct beam solar radiation
f_{dif}: fraction of diffuse solar radiation
s_{sp}: shape factor = 1/(4cos(z)) where z: zenith angle
α_{es}: surface albedo
ε_a: atmospheric emissivity
α_{spl}: globe albedo for longwave radiation = 0.05
σ: Stefan-Boltzmann Constant = 5.67 x 10^{-8} W/m^{2}K^4
T_a: air temperature (Celsius)
ε_g: globe thermal emissivity = 0.95
T_g: Black-globe Temperature (Celsius)
u: wind speed (m/hr)

Appendix B

Methodology Flow Chart

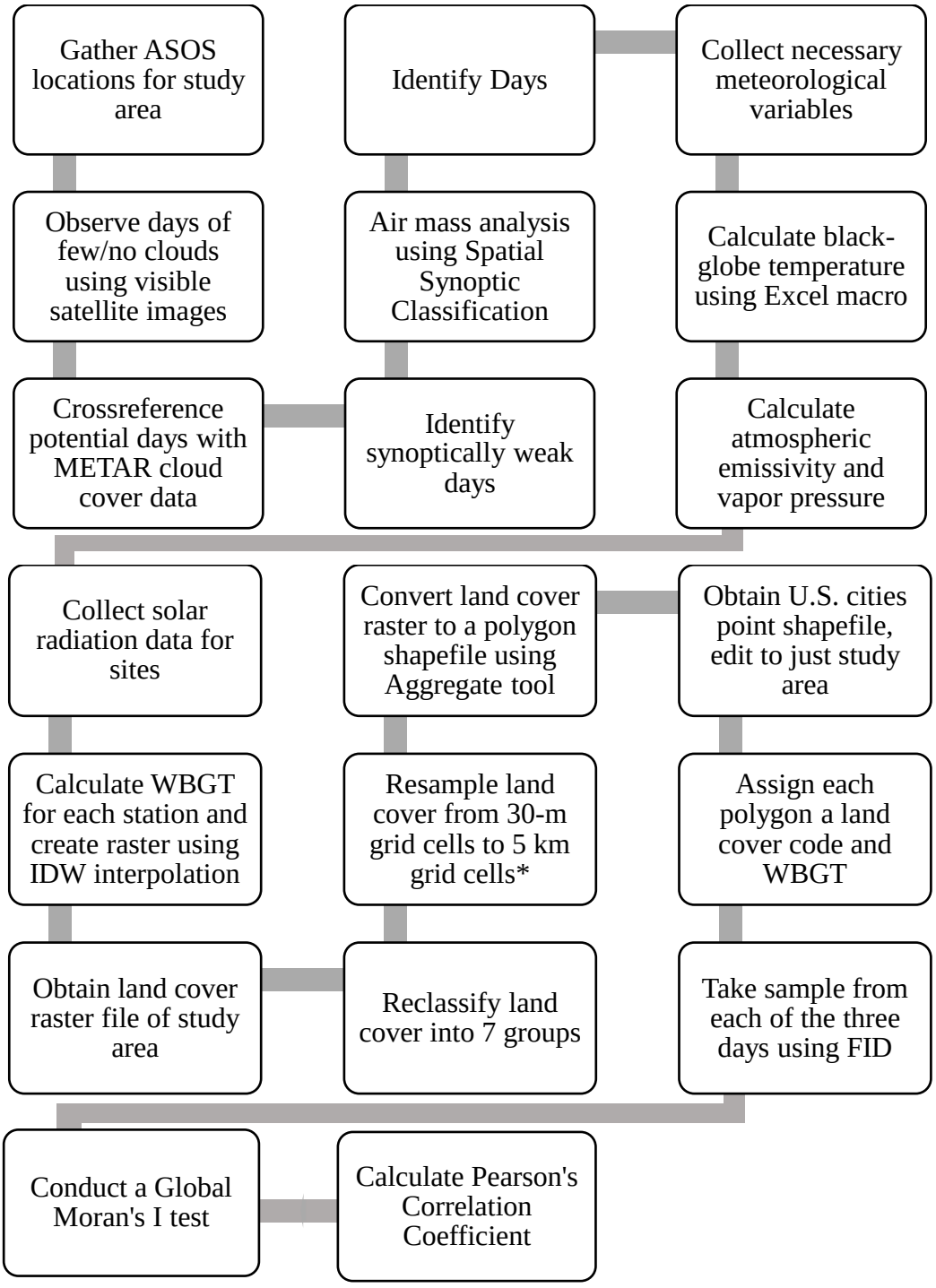

*****This step is done twice to obtain 2 layers, one that remains LULC and one that is converted to a polygon shapefile

References

Ahijevych, D., 1999: Image Archive. Meteorlogical case study selection kit. UCAR/NCAR/MMM.

Akbar-Khanzadeh, F., and J. D. Ramsey, 1987: The Prediction of Temperatures and Heat Stress Limits in the Workplace with Natural Ventilation. *AIHA Journal*, **48,** 396-399.

Alfano, F. R. D. A., B. I. Palella, and G. Riccio, 2012: On the Problems Related to Natural Wet Bulb Temperature Indirect Evaluation for the Assessment of Hot Thermal Environments by Means of WBGT. *The Annals of Occupational Hygiene* **56,** 1063.

Anderson, G. B., and M. L. Bell, 2011: Heat Waves in the United States: Mortality Risk during Heat Waves and Effect Modification by Heat Wave Characteristics in 43 U.S. Communities. *Environmental Health Perspectives*, **119,** 210-218.

Anderson, J. R., E. E. Hardy, J. T. Roach, and R. E. Witmer, 1976: A Land Use and Land Cover Classification System for Use with Remote Sensor Data. *USGS Prof Paper 964*.

Baldwin, R.: NNDC Climate Data Online. Global Summary of the Day. NOAA/NCDC.

Belcher, B. N., and A. T. DeGaetano, 2007: A Revised Empirical Model to Estimate Solar Radiation Using Automated Surface Weather Observations. *SOLAR ENERGY*, **81,** 329-345.

Bergeron, M. F., and Coauthors, 2012: International Olympic Committee Consensus Statement on Thermoregulatory and Altitude Challenges for High-level Athletes. *British Journal of Sports Medicine* **46,** 770.

Bernard, T. E., and M. Pourmoghani, 1999: Prediction of workplace wet bulb global temperature. *Applied occupational and environmental hygiene*, **14,** 126.

Bernard, T. E., and C. A. Barrow, 2013: Empirical Approach to Outdoor WBGT from Meteorological Data and Performance of Two Different Instrument Designs. *Industrial Health*, **51,** 79.

Bernard, T. E., and I. Iheanacho, 2015: Heat Index and Adjusted Temperature as Surrogates for Wet Bulb Globe Temperature to Screen for Occupational Heat Stress. *Journal of Occupational and Environmental Hygiene*, **12,** 323.

Bernard, T. E., V. Caravello, S. W. Schwartz, and C. D. Ashley, 2008: WBGT Clothing Adjustment Factors for Four Clothing Ensembles and the Effects of Metabolic Demands. *Journal of occupational and environmental hygiene*, **5,** 1.

Bonan, G. B., 2001: Observational Evidence for Reduction of Daily Maximum Temperature by Croplands in the Midwest United States. *Journal of Climate*, **14,** 2430-2442.

Botsford, J. H., 1971: A wet globe thermometer for environmental heat measurement. *American Industrial Hygiene Association journal*, **32,** 1.

Brocherie, F., and G. P. Millet, 2015: Is the Wet-Bulb Globe Temperature (WBGT) Index Relevant for Exercise in the Heat? *Sports Medicine*, **45,** 1619-1621.

Bröde, P., and Coauthors, 2012: Deriving the Operational Procedure for the Universal Thermal Climate Index (UTCI). *International Journal of Biometeorology*, **56,** 481-494.

Budd, G. M., 2008: Wet-bulb globe temperature (WBGT)--its history and its limitations. *Journal of science and medicine in sport / Sports Medicine Australia*, **11,** 20.

United States Census Bureau, 2014: 2014 TIGER/Line Shapefiles. US Census Bureau.

Buyantuyev, A., and J. Wu, 2010: Urban Heat Islands and Landscape Heterogeneity: Linking Spatiotemporal Variations in Surface Temperatures to Land-cover and Socioeconomic Patterns. *Landscape Ecology*, **25,** 17-33.

Cadarette, B. S., S. J. Montain, M. A. Kolka, L. A. Stroschein, and W. T. Matthew, 1996: Evaluation of USARIEM Heat Strain Model: MOPP Level, Exercise Intensity in Desert and Tropic Climates. United States Army Research Institute of Environmental Medicine, Ed.

Cadarette, B. S., S. J. Montain, M. A. Kolka, L. Stroschein, W. Matthew, and M. N. Sawka, 1999: Cross validation of USARIEM heat strain prediction models. United States Army Research Institute of Environmental Medicine. *Aviation, Space, and Environmental Medicine*, **70,** 996.

Carlson, T. N., and S. T. Arthur, 2000: The Impact of Land use — Land Cover Changes due to Urbanization on Surface Microclimate and Hydrology: A Satellite Perspective. *Global and Planetary Change*, **25,** 49-65.

Cermak, V., L. Bodri, M. Kresl, P. Dedecek, and J. Safanda, 2016: Eleven Years of Ground-air Temperature Tracking over Different Land Cover Types: Ground-Air Temperature Tracking. *International Journal of Climatology*.

Cheng, F.-Y., Y.-C. Hsu, P.-L. Lin, and T.-H. Lin, 2013: Investigation of the Effects of Different Land Use and Land Cover Patterns on Mesoscale Meteorological Simulations in the Taiwan Area. *Journal of Applied Meteorology and Climatology*, **52,** 570-587.

Ciriello, V. M., and S. H. Snook, 1977: The prediction of WBGT from the Botsball. *American Industrial Hygiene Association journal*, **38,** 264.

Dai, A., K. E. Trenberth, and T. R. Karl, 1999: Effects of Clouds, Soil Moisture, Precipitation, and Water Vapor on Diurnal Temperature Range. *Journal of Climate*, **12,** 2451-2473.

Dernedde, E., and D. Gilbert, 1991: Prediction of Wet-Blulb Globe Temperatures in Aluminum Smelters. *American Industrial Hygiene Association Journal*, **52,** 120-126.

Dimiceli, V. E., S. F. Piltz, and S. A. Amburn, 2011: Estimation of Black Globe Temperature for Calculation of the Wet Bulb Globe Temperature Index. *Lecture Notes in Engineering and Computer Science*, **2194,** 591-599.

Durre, I., and J. M. Wallace, 2001: The Warm Season Dip in Diurnal Temperature Range over the Eastern United States. *Journal of Climate*, **14,** 354-360.

Emes, J., C. K. Redmond, P. C. Magee, and E. Kamon, 1978: Models for Estimating Worksite WBGT. *American Industrial Hygiene Association journal*, **39,** 592.

EPA, 2016a: Heat-Related Illnessess. United States Environmental Protection Agency, Ed., 6.

——, 2016b: Heat-Related Deaths. United States Environmental Protection Agency, Ed., 6.

Epstein, Y., and D. S. Moran, 2006: Thermal Comfort and the Heat Stress Indices. *Industrial Health*, **44,** 388-398.

Department of the Army, Navy, and Air Force, 1957.

Fry, J. A., and Coauthors, 2011: Completion of the 2006 national land cover database for the conterminous United States. *Photogrammetric engineering and remote sensing*, **77,** 858-864.

Gallo, K. P., D. R. Easterling, and T. C. Peterson, 1996: The Influence of Land Use Land Cover on Climatological Values of the Diurnal Temperature Range. *Journal of Climate*, **9,** 2941-2944.

Gaspar, A. R., and D. A. Quintela, 2009: Physical Modelling of Globe and Natural Wet Bulb Temperatures to Predict WBGT Heat Stress Index in Outdoor Environments. *International Journal of Biometeorology*, **53,** 221-230.

Gonzalez, R. R., G. N. Sexton, and K. B. Pandolf, 1985: Biophysical Evaluation of the Wet Globe Temperature Index (Botsball) at High Air Movements and Constant Dew Point Temperature. United States Army Research Institute of Environmental Medicine, Ed.

Graham, S., cited 2016: Land Cover Classification. [Available online at http://earthobservatory.nasa.gov/Features/LandCover/printall.php.]

Graumann, A., 2003: Data Documentation for Dataset 3701, GOES Data User's Guide, ver 1.1. *Ashville, NC: National Climatic Data Center*.

Grossman-Clarke, S., J. A. Zehnder, T. Loridan, and C. S. B. Grimmond, 2010: Contribution of Land Use Changes to Near-Surface Air Temperatures during Recent Summer Extreme Heat Events in the Phoenix Metropolitan Area. *Journal of Applied Meteorology and Climatology*, **49,** 1649-1664.

Grossman-Clarke, S., J. A. Zehnder, W. L. Stefanov, Y. Liu, and M. A. Zoldak, 2005: Urban Modifications in a Mesoscale Meteorological Model and the Effects on Near-Surface Variables in an Arid Metropolitan Region. *Journal of Applied Meteorology*, **44,** 1281-1297.

Heisler, G. M., A. Ellis, D. J. Nowak, and I. Yesilonis, 2016: Modeling and Imaging Land-cover Influences on Air Temperature in and near Baltimore, MD. *Theoretical and Applied Climatology*, **124,** 497-515.

Herzmann, D., 2001: Iowa Environmental Mesonet Archive. ASOS-AWOS-METAR Data Download Archive.

Hunter, C. H., 1999: Estimating Wet Bulb Globe Temperature Using Standard Meteorological Measurements.

Jendritzky, G., G. Havenith, P. Weihs, E. Batschvarova, and R. DeDear, 2008: The Universal Thermal Climate Index UTCI–Goal and State of COST Action 730. *18th International Conference on Biometeorology, Tokyo*.

Juang, Y.-J., and Y.-C. Lin, 2007: The Effect of Thermal Factors on the Measurement of Wet Bulb Globe Temperature. *Journal of Occuopational Safety and Health*, **15,** 191-203.

Lemke, B., and T. Kjellstrom, 2012: Calculating Workplace WBGT from Meteorological Data: A Tool for Climate Change Assessment. *Industrial Health*, **50,** 267-278.

Lengfeld, K., U. G. Feister, and A. Macke, 2010: Parameterization of Solar Radiation from Model and Observations. *Meteorologische Zeitschrift*, **19,** 25-33.

Liljegren, J. C., R. A. Carhart, P. Lawday, S. Tschopp, and R. Sharp, 2008: Modeling the Wet Bulb Globe Temperature Using Standard Meteorological Measurements. *Journal of Occupational and Environmental Hygiene*, **5,** 645-645.

Lu, D., and Q. Weng, 2006: Spectral Mixture Analysis of ASTER Images for Examining the Relationship Between Urban Thermal Features and Biophysical Descriptors in Indianapolis, Indiana, USA. *Remote Sensing of Environment*, **104,** 157-167.

Macpherson, R. K., 1962: The Assessment of the Thermal Environment a Review. *British Journal of Industrial Medicine*, **19,** 151-164.

Maia, P. A., Á. C. Ruas, and D. P. Bitencourt, 2013: Wet-bulb Globe Temperature Index Estimation Using Meteorological Data from São Paulo State, Brazil. *International Journal of Biometeorology,* **59,** 1395-1403.

Malchaire, J., B. Kampmann, G. Havenith, P. Mehnert, and H. J. Gebhardt, 2000: Criteria for Estimating Acceptable Exposure Times in Hot Working Environments: A Review.

Malchaire, J., and Coauthors, 2001: Development and Validation of the Predicted Heat Strain Model. *The Annals of Occupational Hygiene,* **45,** 123-135.

Malchaire, J. B., 1976: Evaluation of Natural Wet Bulb and Wet Globe Thermometers. *The Annals of Occupational Hygiene,* **19,** 251.

Matthew, W. T., W. R. Santee, and L. G. Berglund, 2001: Solar Load Inputs for USARIEM Thermal Strain Models and the Solar Radiation-Sensitive Components of the WBGT Index.

Matthew, W. T., L. G. Berlund, W. R. Santee, and R. R. Gonzalez, 2003: USRIEM Heat Strain Model: New Algorithms Incorporating Effect of High Terrestrial Altitude.

Maxwell, E. L., 1998: METSTAT—The Solar Radiation Model used in the Production of the National Solar Radiation Data Base (NSRDB). *Solar Energy,* **62,** 263-279.

Moran, D. S., and K. B. Pandolf, 1999: Wet Bulb Globe Temperature (WBGT)--to what Extent is GT Essential? *Aviation, Space, and Environmental Medicine,* **70,** 480.

Moran, D. S., and Y. Epstein, 2006: Evaluation of the Environmental Stress Index (ESI) for Hot/Dry and Hot/Wet Climates. *Industrial Health*, **44,** 399-403.

Moran, D. S., A. Laor, Y. Epstein, and Y. Shapiro, 1998: A Modified Discomfort Index (MDI) As a substitutde for the Wet Bulb Globe Temperature (WBGT). *Medicine & Science in Sports & Exercise*, **30,** 284.

Moran, D. S., K. B. Pandolf, Y. Shapiro, Y. Heled, Y. Shani, W. T. Mathew, and R. R. Gonzalez, 2001a: An Environmental Stress Index (ESI) as a Substitute for the Wet Bulb Globe Temperature (WBGT). *Journal of Thermal Biology*, **26,** 427-431.

Moran, D. S., and Coauthors, 2001b: The Role of Global Radiation Measured by a Light Sensor on Heat Stress Assessment. *Journal of Thermal Biology*, **26,** 433-436.

Oke, T. R., 1987: *Boundary Layer Climates.* Vol. 2nd;2nd;, Routledge Ltd - M.U.A.

Perez, R., P. Ineichen, K. Moore, M. Kmiecik, C. Chain, R. George, and F. Vignola, 2002: A new operational model for satellite-derived irradiances: Description and validation. *SOLAR ENERGY*, **73,** 307-317.

Plunkett, J. M., and R. P. Carter, 1974: Practical Problems in the Use of WBGT for Heat Stress Evaluation. *American Industrial Hygiene Association journal*, **35,** 282.

Pryor, S. C., D. Scavia, M. Downer, L. Gaden, R. Iverson, J. P. Nordstron, and G. P. Roberston, 2014: Ch. 18: Midwest. *Climate Changes in the United States: The Third National Assessment*, J. M. Melillo, T. C. RIchmond, and G. W. Yohe, Eds., U.S. Global Change Research Program, 418-440.

Qu, R., X. Cui, H. Yan, E. Ma, and J. Zhan, 2013: Impacts of Land Cover Change on the Near-Surface Temperature in the North China Plain. *Advances in Meteorology,* **2013,** 1-12.

Santee, W. R., and R. F. Wallace, 2005: Comparison of Weather Service Heat Indices Using a Thermal Model. *Journal of Thermal Biology*, **30,** 65-72.

Scheitlin, K. N., and P. G. Dixon, 2010: Diurnal Temperature Range Variability due to Land Cover and Airmass Types in the Southeast. *Journal of Applied Meteorology and Climatology*, **49,** 879-888.

Sequera, P., J. E. González, K. McDonald, R. Bornstein, and D. Comarazamy, 2015: Combined Impacts of Land Cover Changes and Large-scale Forcing on Southern California Summer Daily Maximum Temperatures. *Journal of Geophysical Research: Atmospheres,* **120,** 9208-9219.

Sheridan, S. C., 2002: The redevelopment of a weather- type classification scheme for North America. *International Journal of Climatology*, **22,** 51-68.

Sohar, E., J. Tennenbaum, and N. Robinson, 1962: A Comparison of the Cumulative Discomfort Index (Cum DI) and Cumulative Effective Temperature (Cum ET), as Obtained by Meteorological Data. *Biometeorology, Tromp SW (Ed.),* 395-400.

Stabler, L. B., C. A. Martin, and A. J. Brazel, 2005: Microclimates in a Desert City were Related to Land Use and Vegetation Index. *Urban Forestry & Urban Greening*, **3,** 137-147.

International Organization of Standardization, 1989: Hot environments: estimation of the heat stress on working man, based on the WBGT-Index (Wet Bulb Globe Temperature).

——, 2004: Ergonomics of the thermal environment -- Analytical determination and interpretation of heat stress using calculation of the predicted heat strain.

Steadman, R. G., 1979a: The Assessment of Sultriness. Part II: Effects of Wind, Extra Radiation and Barometric Pressure on Apparent Temperature. *Journal of Applied Meteorology,* **18,** 874-885.

——, 1979b: The Assessment of Sultriness. Part I: A Temperature-Humidity Index Based on Human Physiology and Clothing Science. *Journal of Applied Meteorology,* **18,** 861-873.

Thom, E. C., 1959: The Discomfort Index. *Weatherwise*, **12,** 57-61.

Thompson, E. S., 1976: Computation of Solar rRdiation from Sky Cover. *Water Resources Research*, **12,** 859-865.

Tomanovich, A., 2008: POLYNOM.xls

Tonouchi, M., K. Murayama, and M. Ono, 2006: WBGT Forecast for Prevention of Heat Stroke in Japan. *Sixth Symposium on the Urban Environment. AMS Forum: Managing our Physical and Natural Resources: Successes and Challenges JP1*.

Turner, W. D., and A. Mujahid, 1984: The Estimation of Hourly Global Solar Radiation Using a Cloud Cover Model Developed at Blytheville, Arkansas. *Journal of Climate and Applied Meteorology*, **23,** 781-786.

Vancutsem, C., P. Ceccato, T. Dinku, and S. J. Connor, 2010: Evaluation of MODIS Land Surface Temperature Data to Estimate Air Temperature in Different Ecosystems over Africa. *Remote Sensing of Environment*, **114,** 449-465.

Watkins, R., J. Palmer, and M. Kolokotroni, 2007: Increased Temperature and Intensification of the Urban Heat Island: Implications for Human Comfort and Urban Design. *Built Environment*, **33,** 85-96.

Weng, Q., D. Lu, and J. Schubring, 2004: Estimation of Land Surface Temperature–Vegetation Abundance Relationship for Urban Heat Island Studies. *Remote Sensing of Environment*, **89,** 467-483.

Wierks, K., cited 2016: Coroner says Pike High School football player died of heat stroke. [Available online at http://fox59.com/2015/10/15/coroner-says-pike-high-school-football-player-died-of-heat-stroke/.]

Wilcox, S., 2012: National Solar Radiation Database 1991–2010 update. *National Renewable Energy Laboratory, US Department of Energy*.

Yaglou, C. P., and D. Minard, 1957: Control of Heat Casualties at Military Training Centers. *A.M.A. Archives of Industrial Health* **16,** 302.